ADVANCED TECHNOLOGY FOR INFILL AND RECOMPLETION CANDIDATE WELL SELECTION

Final Technical Report

Reporting Period Start Date: September 1, 2004
Reporting Period End Date: December 31, 2005

By
Duane A. McVay
Walter B. Ayers, Jr.
Yueming Cheng
Jianwei Wang

July 2006

DE-FC26-04NT42098
Subcontract No. 2772-TAMU-DOE-2098

Department of Petroleum Engineering
Texas A&M University
3116 TAMU
College Station, Texas 77843-3116

DISCLAIMER

ABSTRACT

The goal of this project was to develop and demonstrate advanced technology for rapid, cost-effective and reliable assessment of infill drilling and recompletion potential in stripper gas well fields. In this study, we developed an improved simulation-based regression technique to assess infill drilling potential in stripper gas well fields. With limited, basic reservoir information, this technique first estimates the spatial distribution of subsurface reservoir properties by rapid history matching of well production data. We implemented a sequential regression algorithm to estimate not only the permeability distribution, but also the pore volume distribution from available flow rate measurements. Future production is forecast and infill drilling potential is determined using the estimated permeability and pore volume distributions.

The improved technology was validated in a synthetic stripper gas reservoir and in the Second White Specks (SSPK) formation, Garden Plains field, Western Canada Sedimentary Basin. The Garden Plains SSPK field qualifies as a stripper gas field and has approximately 772 non-commingled gas wells with cumulative production of 45.9 Bcf through 2004. To characterize Garden Plains field, we analyzed SSPK well logs, core reports, and production data and made structural, isopach, net sandstone thickness, porosity, permeability, and production maps. In validating the new technology, we found that sequential inversion of both porosity-thickness and permeability results in a significant improvement in matches of predicted performance of both existing and infill wells, as compared to inversion of permeability only as in the previous technology.

Importantly, history matches and performance predictions generated starting with a homogeneous geological model were similar to history matches and performance predictions generated starting with a detailed prior geological model. This validates the use of the technology in situations in which a detailed geological model is not available. The simulation-based inversion technology provides rapid, reliable and cost-effective assessment of infill and redevelopment potential in stripper gas well fields. This approximate approach can provide a rapid, less-expensive alternative to conventional integrated reservoir studies for determining infill and recompletion potential, and can serve as a valuable reservoir management tool for operators of marginal stripper fields.

TABLE OF CONTENTS

LIST OF TABLES

LIST OF FIGURES (Located at end of report)

EXECUTIVE SUMMARY

The objectives of this research were to develop and demonstrate advanced technology for rapid, cost-effective and reliable assessment of infill drilling and recompletion potential in stripper gas well fields. Often, it is difficult to quantify the redevelopment potential of marginal oil and gas fields due to a wide range of depositional environments, variability in reservoir properties, large numbers of wells, and limited reservoir information. With traditional simulation methods, evaluation of infill potential for these fields is time consuming, labor intensive and frequently cost-prohibitive. Without adequate assessment technology, some unprofitable infill campaigns may be initiated while other promising infill campaigns may be terminated prematurely due to disappointing early results.

In this study, we developed an improved simulation-based regression technique to assess infill drilling potential in stripper gas well fields. With limited, basic reservoir information, this technique first estimates the spatial distribution of subsurface reservoir properties by rapid history matching of well production data. We implemented a sequential regression algorithm to estimate not only the permeability distribution, but also the pore volume distribution from available flow rate measurements. Future production is forecast and infill drilling potential is determined using the estimated permeability and pore volume distributions. Because the method employs an approximate reservoir description, it identifies regions of the field with promising infill potential rather than individual infill well locations.

The new technology was first validated in a synthetic stripper gas reservoir. The improved technology was able to reproduce the main features of heterogeneous porosity-thickness and permeability distributions. Including inversion of porosity-thickness with the permeability inversion results in a significant reduction in errors in predicted performance of both existing and infill wells, as compared to previous versions of the simulation-based technology in which only permeability was inverted.

The new technology was also validated in Garden Plains field, Western Canada Sedimentary Basin. Garden Plains field was discovered in 1979 and has approximately 772 gas wells that produce solely from the Second White Specks (SSPK) formation. Cumulative production from these wells through 2004 was 45.9 Bcf. Garden Plains SSPK field qualifies as a stripper gas field; average production is less than 60 Mcf/d/well.

Garden Plains field is the northern-most gas field that produces from the SSPK. To characterize the SSPK reservoirs in Garden Plains field, we used well logs, core reports, and production data to make structural, isopach, net sandstone thickness, porosity, permeability, and production maps. In Garden Plains field, SSPK is a shallow formation (2,478 – 3,423 ft; 760-1050 m deep) composed of calcareous, very fine-grained, shaly sandstone with sandy shale interbeds. Dip of the SSPK formation is less than 1° westward. Structural relief across the field is 350 ft (107 m), and a gas/water contact was not identified. Using well-log facies analysis, we subdivided the SSPK formation into four units, Units A – D, base to top. Units A and B are the primary gas producing units.

They extend more than 40 mi (64 km) east-northeastward and are more than 20 mi (32 km) wide. Unit A has average gross thickness of 15 ft (4.6 m) and, generally, it has better reservoir quality and lateral continuity than Unit B. Unit B has more complex log facies and averages 10 ft (3.2 m) thick. Using net sand cutoffs of 8% porosity and 105 API units on the gamma ray curve (V_{sh}), average reservoir porosity ranges from 8.9 to 14.8% for Unit A and from 7.6 to 14.6% for Unit B. Permeability ranges from 0.18 to 0.96 md for Unit A and from 0.05 to 1.17 md for Unit B.

Evaluation of SSPK core data demonstrated a good relation between porosity and permeability. Porosity-net-thickness product, and by relation permeability, appear to exert the greatest control on production from SSPK reservoirs in Garden Plains field. Structural position, minor structural features, and spud date (initial reservoir pressure) exercise secondary control on production.

In validating the new simulation-based regression technology in the Garden Plains SSPK reservoir, we found that inversion of both porosity-thickness and permeability results in a significant improvement in matches of predicted performance of both existing and infill wells, as compared to inversion of permeability only, as in the previous technology. In addition, calculated permeability and pore volume distributions, performance predictions and infill assessments generated starting with a homogeneous geological model were similar to property distributions, predictions and infill assessments generated starting with a detailed prior geological model. This validates the use of the technology in situations in which a detailed geological model is not available.

The simulation-based inversion technology provides rapid, reliable and cost-effective assessment of infill and redevelopment potential in stripper gas well fields. Successful validation and assessment of infill potential in the Second White Specks formation, Garden Plains field, which has more than 700 wells, demonstrates the power and utility of the technology.

INTRODUCTION

Infill drilling can be an effective means to accelerate field development, increase field oil/gas production rates, and add reserves. Before implementing any program to increase well density, the potential of infill drilling must be reliably assessed to justify such infill activities both technically and economically, especially for marginal oil and gas fields. Without reliable evaluation of infill potential, some unprofitable infill campaigns may be initiated while other promising infill campaigns may be terminated prematurely due to disappointing early results. Quantification of infill drilling for marginal fields represents a significant technical challenge, not only because of the complexity involved in evaluations due to a wide range of depositional environments and large variability in reservoir properties, but also because evaluations often have to deal with large numbers of wells (e.g., hundreds to thousands), limited reservoir information, and time and budget constraints.

It is well recognized that the performance of infill wells depends on many factors and their interaction. These factors include reservoir heterogeneity or spatial variations of reservoir properties (such as permeability, net pay, porosity and gas saturation), well interference, and available reservoir energy (pressure). The combination or interaction of these factors determines how much oil/gas can be produced in the future. These factors and their interaction must be well understood and adequately evaluated to provide reliable assessment of infill drilling potential. To achieve this, assessment technology must be able to address the above engineering concerns and, at same time, must be cost-effective and able to handle the practical issues of large numbers of wells and limited reservoir information.

In general, an integrated reservoir study, which typically requires detailed geological, geophysical, petrophysical, reservoir engineering and reservoir simulation studies, is the best way to evaluate infill drilling potential. Integrated reservoir studies can adequately address the engineering concerns discussed above. However, for marginal fields, high costs and the lack of relevant reservoir data make such detailed studies difficult to perform and economically unjustifiable. One of key tasks in a reservoir simulation study is calibrating the reservoir model by matching the historical production data. It is very challenging and time consuming to achieve a history match in a field with hundreds or thousands of wells in a traditional simulation study.

In the past decade, some authors have proposed statistical moving window techniques to provide rapid and cost-effective assessment of infill drilling potential in large tight gas fields.[1-3] These techniques perform statistical analyses of production data using defined performance indicators, such as the best 12 consecutive months of production and decline ratio for the best year. The performance indicators serve as proxies for reservoir properties, production response and reservoir pressure. Based on the comparison of indicators between old wells to new wells in areal “windows” throughout the field, judgments are then made regarding interference between existing wells and whether pressure depletion is occurring. These judgments are then used to estimate the potential for infill drilling in each window. While this technology can be a useful

screening tool to determine which regions of the field have potential for infill drilling, the prediction errors for infill well performance can be quite significant as well interference effects become complicated and reservoir heterogeneity increases.[4]

To improve upon moving window methods, Gao and McVay[5] proposed a simulation-based regression approach for rapid assessment of infill potential in gas well fields. Utilizing readily available data (such as well locations, production data, and field-wide average values of porosity, permeability, saturation and net pay), their approach provides an estimate of the heterogeneous permeability field by inverse modeling. Using the inverted permeability field, the performance of infill wells is predicted. This simulation-based regression approach is demonstrated to result in more accurate predictions of infill performance than moving window statistical methods.[4] However, while their reservoir model takes into account permeability heterogeneity, all other reservoir properties remain fixed at their initial values. Thus, their model does not condition the hydrocarbon pore volume distribution (resulting from the porosity, net thickness, and hydrocarbon saturation distributions) to the production data. In marginal reservoirs, the initial geological model is often based on incomplete data and analyses, and in some cases, may consist of simply constant average values of each reservoir property. Thus, the initial geological model may possess significant errors. Consequently, while infill performance may be predicted more accurately than with moving window methods, because the reservoir model is not able to adjust the pore volume distribution, predictions for infill wells, as well as existing wells, may still contain large errors.[5]

The overall objectives of our research program are to develop and demonstrate advanced technology for rapid, cost-effective and reliable assessment of infill drilling and recompletion potential in stripper well fields. In our previous project for the Stripper Well Consortium, we investigated a simulation-based regression approach for rapid assessment of infill potential in stripper oil well fields.[6] The technology successfully identified infill well locations in synthetic cases, but was unsuccessful in a field case due to problems with the production and injection database and limitations in the commercial regression software that was employed. We recommended that the approach be refined and proven first in gas reservoirs, which are often less complicated than oil reservoirs. These recommendations became the general objectives of this current project. Specifically, the objectives were to extend the simulation-based regression technology to include inversion of the pore volume distribution as well as the permeability distribution, and to demonstrate the increased reliability of the technology in predicting performance and assessing infill potential by application to both synthetic and actual stripper gas reservoirs. In the following sections, we first present the development of the sequential inversion technique to estimate distributions of permeability and pore volume by conditioning to historical production data. Then, we validate this new technique with synthetic and field examples and, finally, demonstrate its application to assess infill potential in the field example.

RESULTS AND DISCUSSION

METHODOLOGY

A practical inverse modeling algorithm is presented in this section. We implemented a sequential inversion of both reservoir permeability and pore volume distributions by integrating production data. Adding pore volume to the regression enhances the quality of the history match, improves the resolution of reservoir characterization, and lays a foundation for reliable prediction of future production performance and assessment of infill drilling potential.

Overview of Rapid Infill Assessment System

Our simulation-based regression technique is a rapid, cost-effective and reliable method for assessment of infill drilling potential in stripper gas well fields. The system consists of three major components: (1) forward modeling; (2) inverse modeling; and (3) prediction and infill assessment.

Forward modeling is conducted by a conventional finite-difference, single-phase gas simulator. The simulator computes individual well and field-wide production responses based on an input static geological model and other relevant reservoir data. However, since the initial geological model is derived from static data only, it often fails to reproduce the production history.

Through inverse modeling, or history matching, the geological model can be reconciled to the dynamic response of the reservoir and, as a result, a reliable reservoir model can be built for predicting future production performance. For inverse modeling we employ an automatic history matching, or optimization, process that continuously adjusts reservoir properties (e.g., permeability and porosity) until the best fit of calculated response to historical production data is achieved. A variety of optimization algorithms have been developed for solving inverse problems. One category is sensitivity-coefficient-based algorithms, which requires the calculation of partial derivatives (sensitivity coefficients) of model responses to model parameters. For our application, we selected the generalized pulse-spectrum technique (GPST) for sensitivity calculation.[7, 8] The sensitivity is obtained by partially differentiating the governing flow equation with respect to gridblock properties, e.g., permeability. Because the sensitivity coefficients are calculated by differentiating the flow equation directly, they can be calculated internally by the simulator during a forward model run. Because the production data used for history matching are available only at gridblocks with wells and only at time steps after wells are put into production, the calculation of sensitivity coefficients is conducted to include only those for gridblocks with wells on production. This algorithm is very efficient for cases where the number of wells is much less than the number of gridblocks, which is usually the case, and under the assumption that the sensitivity of production response at the previous time step with respect to permeability of gridblocks is negligible.

The derivation of the sensitivity coefficient of pressure with respect to permeability has been presented in the literature. [7, 8]

After we have performed the inversion of reservoir properties to establish a reservoir model conditioned to the production response, we can then predict future performance and assess infill drilling potential. First, we make a base case forecast with existing wells. Then, we place a new well in the first grid block of the reservoir model and make a forecast to determine the incremental field production to be gained by a new well in this grid block. We repeat this for each grid block in the system, thus generating a distribution of the additional field production attributable to one new well at all the possible grid locations in the reservoir. An incremental field production map is then generated and used as an indicator for selection of potential infill drilling areas.

The system consisting of forward modeling, inverse modeling, and prediction/infill assessment components has been integrated in a FORTRAN software application. Application software is available from the authors upon request.

Sequential Inversion Algorithm

Reservoir permeability is the most popular parameter for adjustment in inverse modeling, due to its large variation, limited measurement, and significant effect on reservoir response. However, other reservoir properties, such as net thickness, porosity, and gas saturation, are also quite uncertain in areal distribution and can have important influences on production performance, particularly when lumped together as hydrocarbon pore volume. In reservoir characterization by inverse modeling, many studies focus on only the search for a permeability distribution that can best reproduce the observed production history, and they neglect to adjust other reservoir properties such as pore volume. The reservoir model established after history matching on permeability only could result in significant error in prediction of production performance, as shown in Table 5 of Ref. [5], since it may contain an inaccurate characterization of the distribution of pore volume. An uncalibrated pore volume distribution also influences the effectiveness of the permeability inversion, which contributes to inaccuracy in long-term production performance predictions. In other words, an inverted permeability distribution coupled with an uncalibrated pore volume distribution may not be a representative reservoir system for predicting long-term dynamic behavior. It should not be surprising if the actual future production performance deviates significantly from predicted performance.

In this study, we developed a practical inverse modeling algorithm which implements a sequential inversion of both reservoir permeability and pore volume distributions by integrating production data.

Procedure

There are two sets of inverse parameters considered. The first is reservoir permeability. The second is a multiplier that is applied to the initial pore volume distribution, so the parameter that is being inverted is effectively pore volume. The sequential inversion and infill assessment procedure is briefly described as follows.

- Run the forward model and calculate sensitivity coefficients of production response with respect to permeability using the GPST.
- Conduct inverse modeling to estimate the change in permeability required to honor the production data, and update the permeability field correspondingly.
- Run the forward model with the calibrated permeability field and calculate sensitivity coefficients of production response with respect to pore volume using the GPST.
- Conduct inverse modeling to estimate the change in pore volume required to honor the production data, and update the pore volume field correspondingly.
- Iterate between inversion on permeability and pore volume until convergence is achieved.
- Predict future performance and assess infill drilling potential using forward modeling with the inverted permeability and pore volume fields.

Inversion of permeability and pore volume fields is iterative. The iteration can be performed between permeability and pore volume flexibly. For example, we can first perform inversion of permeability with one iteration or an arbitrary number of iterations, and then fix the inverted permeability distribution and perform inversion of pore volume with one iteration or an arbitrary number of iterations. The process always proceeds with the latest updated permeability and pore volume fields, and it is repeated until convergence is achieved.

In our studies of marginal gas fields, we find that reservoir pressure data are often limited and that wells often operate at capacity production with line pressures that do not vary significantly with time. Thus, in our inversion, we do not constrain wells at constant rate production and match on pressures, as is usually done. Instead, we constrain wells at constant flowing bottomhole pressure and match on flow rate. The required sensitivity coefficients are, thus, production rate with respect to reservoir parameters (permeability and pore volume multiplier). In the following section, the sensitivity coefficient of production rate with respect to pore volume multiplier is presented. The derivation of the sensitivity coefficient for production rate with respect to permeability is presented in Refs. [5, 7, 8].

Sensitivity Coefficient with Respect to Pore Volume Multiplier

The linear system of flow equations is

$$A\mathbf{p} = \mathbf{b} \quad \text{.....(1)}$$

where **A** is the coefficient matrix of the system, **p** is the vector of gridblock pressures, and **b** represents the right-hand-side term.

The pore volume of the *i*-th gridblock at the *n*-th time step is

$$V_{p,i}^{n} = \left(\Delta x \Delta y h \phi^{n} s_{g}^{n}\right)_{i}, \quad \text{.....(2)}$$

where $V_{p,i}$ is the hydrocarbon pore volume of the *i*-th gridblock, Δx and Δy are gridblock dimensions, h is the gridblock net thickness, ϕ is porosity, S_g is gas saturation, and the superscript n signifies the n-th time step. In the following discussion, the hydrocarbon pore volume is simply denoted as pore volume for the convenience of presentation. The initial pore volume distribution is defined with estimated average reservoir properties or a prior geological model. For purposes of inverting pore volume, we define a pore volume multiplier, β. The initial value of β for all gridblocks is 1 and is calibrated by history matching of production data. Pore volume for the *i*-th gridblock is updated in the history matching process and can be expressed as:

$\beta_i V_{p,i}^{n}$.

To obtain the sensitivity coefficient, we start by taking the partial differential of Eq. 1 with respect to pore volume multiplier of the *i*-th gridblock,

$$\frac{\partial \mathbf{p}}{\partial \beta_i} = A^{-1}\left(\frac{\partial \mathbf{b}}{\partial \beta_i} - \frac{\partial A}{\partial \beta_i}\mathbf{p}\right). \quad \text{.....(3)}$$

As mentioned before, we only need to know the sensitivity coefficients at the gridblocks with wells. Using a vector $\boldsymbol{\beta}$ to represent the pore volume multipliers of all gridblocks, we then can express the sensitivity coefficients of pressure in the gridblock with a well to $\boldsymbol{\beta}$ as

$$\frac{\partial p_l}{\partial \boldsymbol{\beta}} = \mathbf{C}_{\alpha}\mathbf{x}, \quad \text{.....(4)}$$

where **X** is the *l*-th row of $\mathbf{A}^{-1}$, and subscript l represents the *l*-th gridblock, which contains a well. $\boldsymbol{C_{\alpha}}$ is a diagonal matrix, and the *i*-th element on the diagonal of this matrix is

$$C_{\alpha,i} = \alpha_i \left(p_i^{n-1} - p_i^{n}\right), \quad \text{.....(5)}$$

where superscript n represents the time step, and α is defined as:[9]

$$\alpha_i = \frac{1}{\Delta t}\frac{T_{sc}}{p_{sc}T}\frac{\left(\frac{V_p p}{Z}\right)_i^{n} - \left(\frac{V_p p}{Z}\right)_i^{n-1}}{p_i^{n} - p_i^{n-1}}. \quad \text{.....(6)}$$

Taking the partial derivative of the well equation in the simulator,

$$q_l = J(p_l^n - p_{wf}), \quad \text{.....(7)}$$

we obtain the sensitivity coefficient of production rate with respect to $\boldsymbol{\beta}$

$$\frac{\partial q_l}{\partial \boldsymbol{\beta}} = J \frac{\partial p_l}{\partial \boldsymbol{\beta}}, \quad \text{.....(8)}$$

where J is productivity index.

Inversion—Optimization Process

As mentioned before, inversion consists of an optimization process either for permeability or for pore volume. The optimization process can be described as the minimization of the objective function, which is the sum of the squares of the data residuals. Eq. 9 is the expression of the objective function.

$$J = \|\delta \mathbf{d} - \mathbf{S}\delta \mathbf{R}\| = \sum_{i=1}^{n} \left(\delta d_i - \sum_{j=1}^{m} S_{ij}\delta R_j\right)^2, \quad \text{.....(9)}$$

where || || denotes the L2 norm of a vector; $\delta\mathbf{d}$ is the residual vector, that is the difference between the observed and calculated dynamic data (flow rate or pressure); **S** symbolizes the sensitivity matrix that quantifies the change in predicted responses due to a change in reservoir properties, such as permeability or pore volume; and $\delta\mathbf{R}$ is the reservoir property change vector—parameters being evaluated in the inversion. In this research, we invert both permeability and pore volume, and solve the associated inverse problem iteratively.

The inverse problem is ill-posed, as a number of parameters (distribution of permeability or pore volume) are involved. To stabilize the inverse problem, in general, two additional penalty terms are included in the objective function for regularization.

$$J = \|\delta \mathbf{d} - S\delta \mathbf{R}\| + \beta_1 \|\delta \mathbf{R}\| + \beta_2 \|\mathbf{L}\delta \mathbf{R}\|, \quad \text{.....(10)}$$

where the first added term (the second term on the right-hand side of Eq. 10) is the "norm" constraint, used to penalize large deviations of reservoir properties from the initial model. This assumes that the initial, or prior, model already contains the available geological and static information for the reservoir. The second added term (the third term on the right-hand side of Eq. 10) is the "smoothness" constraint, used to penalize models with excessive spatial property variations. **L** is a spatial difference operator, and β_1 and β_2 are two user-specified weighting factors controlling the relative strengths of the norm term and the smoothness term.

An extremely sparse linear system of equations can be obtained from Eq. 10. To efficiently solve this system, an iterative sparse-matrix solver, LSQR[10], has been used. The LSQR algorithm uses only the nonzero element of the sensitivity matrix and is quite stable.[11]

Other Improvements to Simulation-Based Regression Model

In addition to adding regression on pore volume, we extended the previous simulation-based regression approach[5] in other ways. For example, in the previous project, the effect of a hydraulic fracture on well performance was modeled simply by a skin factor. Although skin factor can be used to approximate enhancement of the well productivity index, it is usually not adequate in simulation of hydraulically fractured wells, because the hydraulic fracture affects not only the productivity of wells but also the transmissibility around wells, particularly when the hydraulic fracture is long relative to grid block sizes. Consequently, history matching and prediction using the previous simulation-based regression approach produced large errors, as shown in Table 5 of Ref. [5]. In the current project, we consider the effects of hydraulic fractures on enhancements of both well productivity index and transmissibility around wells.

We also refined the reservoir model by considering days-on-line information. Integration of days-on-line information into the reservoir model aimed to capture the actual well productivity since the productivity of wells is related to the average rate over the actual production days, not calendar days.

VALIDATION WITH SYNTHETIC EXAMPLE

In this section, we validate our improved simulation-based regression technology using a synthetic gas field example with heterogeneous permeability and porosity distributions. For a synthetic example, the true reservoir property distributions are known; therefore, the estimated reservoir property distributions can be readily compared to the true distributions. In addition, we validate the new technique by examining the predicted production performance, which is significant when estimating remaining reserves and assessing infill drilling potential.

In this synthetic example, 36 wells are initially produced for 23 years. The objective of the analysis is to determine the potential for 10 infill wells. The synthetic reservoir has heterogeneous permeability and porosity fields. Porosity was distributed normally with a mean of 7.72%. The logarithm of permeability was correlated to porosity, and the permeability field has a mean of 0.74 md. Other reservoir properties, such as net thickness and gas saturation, were assumed to be uniform. Thus, heterogeneity in pore volume reflects the heterogeneity of the porosity field.

In our analysis, we assumed that a prior geological model was not available. We initiated automatic history matching with estimated average values of reservoir

properties. The uniform reservoir permeability and porosity values input in the initial simulation model were 0.1 md and 7.5%, respectively. We used the true net thickness of 15 ft. Fig. 1 shows history matching results for field-wide cumulative production and daily rate by applying both the sequential inversion technique (inversion of permeability and pore volume multiplier) and inversion of permeability only. The blue dots represent the actual observed production data, the pink dots are the results from the sequential inversion technique, and the green dots are the results from inversion of permeability only. Matching on both permeability and pore volume significantly improved the quality of the history match. Fig. 2 shows prediction results for the group of existing wells (the upper set of curves) and the infill well group (the lower set of curves) after history matching. The relative error in cumulative production is greatly reduced, from 23.00% to 5.02% for infill wells and from 12.39% to 0.85% for existing wells. Fig. 3 compares the permeability distribution inverted using the sequential technique to the true permeability distribution, while Fig. 4 makes the same comparison for the ϕ^*h distribution. As demonstrated in these figures, the inverted distributions of permeability and pore volume successfully capture the main features of the true property distributions on a large scale. We do not expect to reproduce the distributions on a small scale, because the production response is an integrated response.

APPLICATION TO A FIELD CASE

A primary objective of the project was to validate the improved simulation-based regression technology on an actual producing stripper gas field. In the following sections, we discuss selection of the field, characterization of the reservoir, validation of the new methodology, and application to assessment of infill drilling potential in the field.

Field Selection

A major task of this project was to (1) gather and review literature and production data for the Viking and other formations that host stripper well fields in the Western Canada Sedimentary Basin with cooperation of MGV Energy (a Quicksilver Resources company), (2) select one formation and one or more fields for study, and (3) collect the production and geological data required for the study. The Viking formation was among to top candidates for this study because it has a long gas production history, hosts many stripper gas wells, and is typical of many low permeability gas reservoirs in Canada and the U.S. In addition, production and reservoir data are easily obtained, and we have conducted previous research on Viking production in a 9-township area in Alberta.

With the assistance of MGV Energy, we collected a production database for the Viking Formation in the Western Canada Sedimentary Basin. There are 22,021 Viking formation completions in the database. We merged all useful data from different files to one data file to facilitate data evaluation. For the evaluation, we considered a stripper well as one that produces 60 thousand standard cubic feet (60 Mcf) of natural gas per day, or less. Further, we assumed that if a well does not have production records in the period from July 2003 to June 2004, the well is a non-producing well. Thus, we used only

the latest 12 months of production rate data, i.e. from July 2003 to June 2004, to calculate an average production rate for each well. On the basis of this assessment, we determined that 64% of the producing Viking wells are stripper wells. After calculating the percentage of stripper wells for every field in the Viking formation, we selected Provost, Killam, Viking-Kinsella, and Wainwright fields as candidates for further study. All four fields have large percentages of stripper wells and relatively large numbers of producing wells. We built a base map of all wells in the Viking formation for these 4 fields to facilitate production analysis. Using this base map, we plotted the distributions of producing, non-producing, and stripper wells in the fields. From these maps, we found that Viking formation stripper wells are more concentrated in the east part of the Provost Field and at the confluence of Killam, Viking-Kinsella and Wainwright fields.

Upon further analysis of Provost, Killam, Viking-Kinsella, and Wainwright fields, which produce from the Viking formation, we recognized problems with their databases, and we enlarged our assessment to include Garden Plains field, which produces from the Second White Specks formation. Among the severe limitations of the Viking fields was the fact that many have commingled production, and production allocation was uncertain. However, in Garden Plains field, the SSPK formation has a high percentage (75%) of stripper wells and, most important, production is not heavily commingled. The reported geologic simplicity and good lateral continuity of the SSPK reservoir within the field made it an attractive candidate for the study. Also, approximately 800 wells have been drilled in the field in the last 8 or 9 years, which provides a somewhat modern database. Therefore, following the review of several Viking fields and Garden Plains SSPK field, we selected Garden Plains field for our study.

Garden Plains field is located in southeast Alberta, approximately 100 miles northeast of Calgary (Fig. 5). It extends from Townships 30-34N, Ranges 11-16W4 and is approximately 40 mi long and 20 mi wide (64 X 32 km). Production and completion data provided by MGV Energy [12] indicate that first production was in April 1979. Of 920 SSPK gas wells listed as having produced between discovery date and December 31, 2004, in Garden Plains field, 772 wells produced from the SSPK only; the remaining 148 wells had commingled production. In August 2004, 741 wells reported gas production, whereas 31 wells had no reported gas production. Condensate yield was very limited from the field. Most wells were hydraulically fractured, and a few wells received acidizing treatments. Few wells have water production records.

The SSPK formation produces gas from Garden Plains and from 17 other fields to the south. The SSPK formation reportedly contains approximately 2 to 3 TCF of natural gas in southern Alberta and southwest Saskatchewan.[13] However, gas production from the SSPK formation has been economic only locally. [14] Despite its economic importance, few geologic studies of the SSPK formation have been published. Three reasons for this neglect are that (1) gas occurs only locally in extensive, distal marine, sheet sands; (2) the SSPK formation is composed of muddy, very fine-grained sand with subtle facies variations that require detailed stratigraphic analysis using a large number of wells; and (3) owing to low production rates, gas wells are marginally economic.

Characterization of Garden Plains (SSPK) Field

The objective of this part of the study was to develop a reservoir characterization model of the SSPK formation in Garden Plains field. This reservoir characterization model was needed to validate the simulation-based approach to rapid assessment of infill drilling potential.

REGIONAL GEOLOGY

Garden Plains field is located on the east flank of the Western Canada Sedimentary Basin (WCSB), (Fig. 5). In the study area, the SSPK formation generally dips approximately 0.1° westward. The SSPK formation is present across much of the Western Canada Sedimentary basin.[15, 16] It occurs in the lower part of the Upper Colorado Group, which was deposited in Late Cretaceous (Turonian) time **(**Fig. 6**)**, when sea level was globally high [17]. It overlies the Belle Fourche formation and is overlain by clastic sediments of the upper part of the Upper Colorado Group. The SSPK formation is composed of interbedded shale and sandstone. According to Glass [18] and Bloch et al. [15], the SSPK sands in southern Alberta and Saskatchewan occur in the uppermost part of the newly defined Belle Fourche formation, and the term Second White Specks formation refers only to the speckled coccolithic shales that overlie the sandy interval of the SSPK formation. However, the name "Bell Fourche formation" has not been adopted for this interval by the oil industry, and the EUB (Energy and Utilities Board, Alberta, Canada) continues the designation "Second White Specks formation." Thus, we will use the terminology of the EUB and industry.

The SSPK formation is named for the abundant calcareous nannofossils that are typically concentrated in white, fine- to very fine-grained, sand-sized fecal pellets. SSPK reservoirs rocks are low-permeability, clay-rich sandstones that are interbedded with sandy shale beds. Reportedly, the SSPK formation serves as both a petroleum source rock [19] and as a reservoir [20]. The formation and adjacent shales are thermally immature, and the gas is reportedly locally generated, biogenic gas. [21]

DATABASE

Production data from 920 wells in Garden Plains field were available for this study. However, of these 920 wells, only 772 wells produce solely from the SSPK; in the remaining 148 wells, SSPK production is commingled with that from other formations. Digital log curves were provided for 173 wells that were located primarily in the middle and northeast parts of Garden Plains field. Raster image log curves were provided for 901 wells, including many of those for which we had digital logs. The geophysical log suite varied among wells but generally included combinations of gamma ray, neutron porosity, caliper, and other curves, including resistivity and density porosity. Although core analysis data were provided for 25 cored wells, only 5 wells had both core analysis data

and digital logs. The core analysis data include porosity, permeability, grain density, water saturation, and lithologic descriptions.

STRATIGRAPHIC AND FACIES ANALYSIS

SSPK Stratigraphy

The Second White Specks formation is composed of very fine-grained sandstone and non-bioturbated, calcareous, organic-rich, shaly and silty units that are distinctive due to the abundance and diversity of marine bioclasts, the foraminiferal assemblage, the predominance of Type II organic matter, and the high total organic content (as great as 12 wt%). [15] Historically, the SSPK formation has been divided into upper and lower Second White Specks stratigraphic units.[22] The main reservoir facies is the lower SSPK, which consists of very fine-grained, muddy sandstones that are 18 to 29 ft (5.5 to 9 m) thick.

To assess the SSPK formation stratigraphy and reservoir characteristics, we divided the SSPK into four stratigraphic units (Units A-D, Fig. 7), which we correlated throughout Garden Plains field, using interlocked strike and dip cross sections. Next, we correlated the SSPK in all other well logs in the field to those picks made in the cross sections, and we made structure and isopach maps.

The base of the SSPK formation (and Unit A) is placed at the base of an upward coarsening sequence that marks the contact of SSPK sandstones with underlying Belle Fourche formation shale (Fig. 7). Unit A is an upward-coarsening sandstone that is capped by a thin (~2 ft; 60 cm thick), low-porosity (high density), high-resistivity zone near the top of unit A. This low-porosity zone is inferred to be tightly cemented with carbonate cement. Typically, Unit B is shaly, upward-fining sandstone that commonly is separated from Unit A by a very thin shale unit (Fig. 7). Further differentiation between Units A and B is based on the observations that Unit A has higher resistivity and lower gamma ray and neutron porosity values than Unit B (Fig. 7). The lower SSPK formation Units A and B are the main gas producing zones in Garden Plains field, as is indicated by high resistivity, low gamma ray, and low neutron porosity (gas effect) values, and by perforation data (Fig. 7).

Bentonite 1 is the boundary between the lower, gas productive SSPK and upper, shalier SSPK that has few perforations (boundary between Units B and C, Fig. 7). In well logs, Bentonite 1 is approximately 1 ft (30 cm) thick and is recognized by (1) very high gamma ray API values, (2) high neutron porosity, and (3) low formation resistivity. Because of its distinctive appearance in well logs, field-wide occurrence, and significance as a time horizon, Bentonite 1 is a good correlation and structural marker.

Unit C includes at least 2 shaly sands that have relatively high gamma ray response, high neutron porosity (shale effect), and low resistivity. These sands are interbedded with shales. Bentonite 2 (Fig. 7) marks the boundary betweens Units C and D in the southwest and central parts of the field, but it thins northward and is absent in the

northeast area. Unit D is a sandy shale interval between Bentonite 2 and the top of the SSPK Formation. In well logs, the top of SSPK formation is placed at the small natural gamma spike at the transition from SSPK shaly sands to a dominantly shale interval in the Colorado Shale Group (Fig. 7).

In Garden Plains field, the SSPK formation dips approximately 0.1 degree westward, as is shown in the Bentonite 1 structure map (Fig. 8). A west-plunging syncline crosses the west-central part of the field. Structural relief on the syncline is approximately 147 ft (45 m). Because the field strikes northeastward, oblique to structural dip, the highest elevation of the SSPK is at the northeast margin of the field (Fig. 8 and Fig. 9). Structural relief across the field is 355 ft (109 m). There is no structural closure in Garden Plains field.

SSPK Reservoir Architecture

Units A and B are the primary gas producers in Garden Plains field. Unit A is an upward coarsening, northeast-trending, lensoid sand body that ranges between 7 and 17 ft (2-5 m) thick and averages 15 ft (4.6 m) thick (Fig. 7 and Fig. 10a). Lateral continuity of the unit is good. Unit B is dominantly upward-fining sand interbedded with shale (Fig. 7). It also trends northeastward, but instead of a lensoid geometry, in Garden Plains field, it forms a sedimentary wedge that thickens from approximately 7 ft (2.2 m) thick on the southeast to 13 ft (4 m) thick on the northwest side of the field (Fig. 10b). Its average thickness is approximately 10.5 ft (3.2 m).

Unit C is 18 to 42 ft (5.5 to 13 m) thick (Fig. 10c). The unit is thickest (as much as 33% thicker) coincident with the west-plunging syncline, indicating that the syncline was forming during deposition of Unit C (compare Fig. 8 and Fig. 10c), whereas isopach maps of Units A and B (Fig. 10a and Fig. 10b) indicate that the syncline was not actively forming during deposition of those units. Unit D strikes northeastward and generally thickens to the northwest (Fig. 10d). It ranges between 20 and 32 ft (6 and 10 m) thick in Garden Plains field. The syncline had minor effect on thickness of Unit D (compare Fig. 8 and Fig. 10d). Although combined thickness of Units C and D is twice the combined thickness of Units A and B, Units C and D have poor reservoir quality, and thus, they are rarely perforated and are less important in understanding performance of SSPK gas wells.

PETROPHYSICAL ANALYSIS

Well Log Normalization

Commonly, well log response within a stratigraphic unit varies across a field, owing to instrument calibration error, acquisition error, differences in borehole environments, and differences in various service company instruments. Therefore, reservoir characterization requires that well logs be normalized. Stratigraphic analysis and reviews of well logs revealed significant variation in quality of log response in the

Garden Plains field. There are marked inconsistencies in gamma ray (GR) readings in Shale B, a marine unit that immediately overlies the SSPK formation, among closely-spaced wells (Fig. 11a). GR readings range from 75 to 150 API units in Shale B. It is critical to normalize GR curves to (1) accurately calculate petrophysical properties of SSPK, such as shale volume, (2) correct shale effect on neutron porosity response, and (3) determine net-sandstone cut-offs.

Preliminary petrophysical analysis showed no relationship between core porosity and neutron porosity of SSPK sandstone Units A and B, owing to the lack of normalization and neutron calibration. To normalize logs in Garden Plains field, we used the method of Shier [23], which is given in the equation,

$$GR_{norm} = R_{\min} + \frac{(R_{\max} - R_{\min})}{(W_{\max} - W_{\min})} * (GR_{\log} - W_{\min}), \quad \ldots\ldots\ldots\ldots(11)$$

where GR_{norm} is the normalized value, GR_{log} is original GR log value, R_{min} and R_{max} are the regional best estimates of the minimum and maximum values of the GR curve in the studied interval, and W_{min} and W_{max} are the corresponding values for each well (Fig. 12).

After log normalization, log readings of closely-spaced wells should be similar in the same stratigraphic interval such as shale, or clean sandstone with consistent fluid composition. After normalizing the SSPK interval in Garden Plains field, the GR response of Shale B ranges between 110 and 130 API units (Fig. 11b), whereas before normalization the range was 75 to 150 API units.

Correction for Shale Effect and Calculation of Shale Content

The most accurate method to calculate shale volume (V_{sh}) of sandstone from well logs is to calibrate GR or SP responses of the logs using shale content values determined from core. Because we did not have core analysis of shale content, we used the following method.

Following GR normalization, sand and shale GR baselines were defined.
First, we calculated GR_{index} as: $GR_{index} = (GR-GR_{min})/(GR_{max}-GR_{min})$, where GR is the log response in the shaly sand, GR_{min} is GR response in a clean sand zone, and GR_{max} is GR response in a 100% shale zone. We selected GR_{min}=70 API and GR_{max}=140 API. Then, we used Clavier's equation (below) to calculate shale content, V_{sh}:

$$V_{sh} = 1.7 - \left[3.38 - (GR_{index} + 0.7)^2\right]^{0.5} \quad \ldots\ldots\ldots\ldots\ldots(12)$$

Correction of Neutron Porosity Shale Effect

High shale content of SSPK sandstone causes the neutron porosity values to be approximately 2-times greater than core porosity values for the same interval (Fig. 13). Therefore, neutron porosity cannot be used directly when evaluating shaly sandstone

reservoirs. To determine porosity using neutron porosity logs, the shale effect must be subtracted from the neutron log response. The equation used to calculate effective neutron porosity (PHIN_E) is:

$PHIN\_E = PHIN - V_{sh} * 0.45$, ……..….(13)

where PHIN is the well log neutron porosity value, and 0.45 is neutron porosity of a 100% shale interval.

Core-Log Data Depth Shift

After correcting the neutron porosity response for shale effect, we analyzed SSPK petrophysical properties of 3 key wells (100012103412W4, 100083403312W4, and 100101603312W4). An important step was to depth shift core data to match well log responses. Initially, core porosity did not match well with effective neutron porosity (Fig. 13a), but after depth shifting core porosity to effective neutron porosity, effective neutron and core porosities match well (Fig. 13b).

RESERVOIR PROPERTIES

Reservoir Porosity

The most prevalent porosity logs in Garden Plains field are neutron logs. Thus, neutron porosity logs were used to evaluate SSPK porosity throughout the field. Initially, there was a poor relationship between core porosity and neutron porosity, owing to lack of data depth match and shaliness of the SSPK sandstones. After depth shifting, we calibrated the effective porosity logs by cross-plotting the effective neutron porosity and core porosity. There was a good relationship between core porosity and effective neutron porosity (Fig. 14a), and thus, we corrected the neutron log readings using the following equation.

$$Porosity = 0.5454 * PHIN\_E + 0.0147 \quad \text{……..….(14)}$$

To verify the accuracy of calculated porosity, we compared the calculated porosity with core porosity (Fig. 14b). The agreement between calculated porosity and core porosity is good. Therefore, we applied the above equation to calculate and map porosity throughout the field.

Using net sand cutoffs of 8% porosity and 105 API units on the gamma ray curve (V_{sh}) (See below, *Cutoff Determinations*), average reservoir porosity ranges from 8.9 to 14.8% for Unit A and from 7.6 to 14.6% for Unit B; mean porosities for the two units are 12.4% and 11.8%, respectively.

Permeability Determination

Core data were evaluated to establish a relation between porosity and permeability (Fig. 15). The relationship between porosity and permeability is given by the equation:

$$\text{Permeability} = 464.69*(\text{Porosity})^{3.3028} \quad \ldots\ldots\ldots\ldots(15)$$

Using net sand cutoffs of 8% porosity and 105 API units on the gamma ray curve (V_{sh}) (See below, *Cutoff Determinations*), average reservoir permeability ranges from 0.18 to 0.96 md for Unit A and from 0.05 to 1.17 md for Unit B; mean permeability values for the two units are 0.54 and 0.35 md, respectively.

Cutoff Determinations

Shale volume and porosity cutoffs were used to determine net sandstone thickness in well logs. Net-sand thickness is defined as that part of the gross rock thickness that contributes to hydrocarbon production. Incorrect cutoffs will result in anomalously high or low calculated reservoir volume. However, there is no universal method for determining the correct cutoff. In this study, we evaluated the effects of a number of possible cutoffs for approximately 168 wells that have digital GR curves, and we defined net sand thickness as those sands intervals having porosity > 8% and gamma ray response <105 API units (equals V_{sh} of 30.7%) (Fig. 16).

SEDIMENTARY FACIES AND RESERVOIR PROPERTIES MAPS

After completing the petrophysical analysis and determining cutoffs, we mapped net sandstone thickness, average porosity, average permeability, and porosity-thickness product of the SSPK Units A and B in Garden Plains field. For some areas of the map (especially in the south) we interpolated reservoir properties in the absence of data, because there were potential infill locations and, thus, it was necessary to characterize reservoir properties.

Net Thickness and Net/Gross Thickness

After applying petrophysical cutoffs, we mapped net thicknesses of Unit A, Unit B, and Units A and B combined (Units A+B) and net/gross thickness of Units A and B (Fig. 17a – Fig. 17e)**.** Although most Garden Plains wells are perforated in Units A and B, Unit A is the SSPK primary reservoir in the Garden Plains field, as is apparent from the following maps and discussion. Reservoir properties of Units C and D were not mapped, owing to the limited number of wells completed in these units.

Net thickness of Unit A ranges between 7 and 15.8 ft (2.1 – 4.8 m) and averages 12.3 ft (3.8 m) (Fig. 17a)**.** The net sandstone thickness map depicts Unit A as a rather continuous, elongate, northeast-trending sand body, as previously shown in the gross thickness map (Fig. 10a). Net/gross ratio of Unit A is 55-95% (average = 85%) (Fig. 17d). The net/gross map shows a strongly developed northwest trend that contrasts with the well developed northeast trend in the net thickness map (compare Fig. 17a and Fig. 17d) and suggests more reservoir heterogeneity than indicated by the net sand map.

Net sandstone thickness of Unit B ranges from 0.5 ft to 9 ft (0.15 – 2.7 m) and averages 4.2 ft (1.3 m) (Fig. 17b). Unit B is 10 to 70% sand (average ~45%) (Fig. 17e). In Unit B, strongly developed northwestward trends are apparent in both the net sandstone thickness and net/gross thickness maps (Fig. 17b and Fig. 17e).

Combined net sandstone thickness of Units A and B (A+B) ranges from 10.5 ft to 22 ft (3.2 – 6.7 m) and averages 16.5 ft (5.1 m) (Fig. 17c). This maps suggests a rather homogeneous, northeast-trending SSPK reservoir, owing to the fact that net thickness of Unit A is generally 2-3 times greater than thickness of Unit B (compare Fig. 17a and Fig. 17b). There is no indication in either the net sandstone or net/gross maps that the syncline which crosses the west-central part of the field (Fig. 8) was active during sedimentation. Sandbody trends appear to be unaffected by that structural feature. However, net/gross (sandstone fraction) maps of both Unit A and B (Fig. 17d and Fig. 17e) indicate greater reservoir heterogeneity than do net sandstone thickness (Fig. 17a and Fig. 17b**)** or the previously described gross thickness maps (Fig. 10a and Fig. 10b**)**. To further assess reservoir heterogeneity, we mapped well log gamma ray patterns (electrofacies) of SSPK Units A and B.

Log Facies

GR well log patterns are indicative of sedimentary facies and the energy of the transporting medium. Commonly, in clastic depositional systems, high-energy facies have larger grain size (low GR values) and greater primary porosity and permeability than do low energy facies (high GR values). Also, the vertical changes in GR response may be indicative of the depositional setting. Both Units A and B have strongly developed northwest trends of the well log facies (Fig. 18a and Fig. 18b). The areas of northwest-trending, high-energy well-log facies (upward fining and upward coarsening facies) coincide with the northwest-trending areas of greater sandstone percentage in the net/gross maps (compare Fig. 18a and Fig. 18b with Fig. 17d and Fig. 17e), reinforcing the conclusion that SSPK reservoirs are more heterogeneous than indicated by net sandstone maps.

Reservoir Porosity and Permeability

Using the petrophysical analysis described above, we calculated and mapped average porosity and average permeability for the combined net sandstone intervals of

Units A+B (Fig. 19a and Fig. 19b, respectively). Comparison of porosity and permeability maps shows coincidence of high and low values, because permeability was derived from the porosity-permeability transform. Porosity and permeability vary considerably across the field, suggesting significant reservoir heterogeneity.

Porosity-Net Thickness Product

To investigate effects of total pore volume on reservoir performance, we mapped the porosity-net-thickness product for the combined net sandstone intervals of Units A+B for each well that had digital log data (Fig. 19c). Porosity-net thickness product of the combined Units A+B ranges between 1.4 and 2.6. Anomalously high and low values of porosity-net-thickness product trend northwestward and northeastward.

GEOLOGIC CONTROLS ON RESERVOIR PERFORMANCE

Production Summary

In Garden Plains field, 772 gas wells have produced gas from the SSPK only. First production in this area was in April 1979. In August 2004, 741 wells reported gas production, whereas 31 wells had no reported gas production. Condensate yield is very limited from the field. Few wells have water production records. In Garden Plains field, 75% of the SSPK gas wells are stripper wells (production < 60 Mcf/d). Cumulative gas production for the field was 45.9 Bcf through December 31, 2004.

To assess geologic controls on reservoir performance, we calculated and mapped values of best year of gas production (BYG) (Fig. 19d), which was defined as average daily gas production during the best consecutive 12 months of production of each well. Also, we plotted values of BYG against the porosity-net thickness product (Fig. 20) and compared the BYG and structure maps (Fig. 19d and Fig. 8). During the best year of production, SSPK average daily gas production from individual wells ranged from 0.7 to 750 Mcf/d (Fig. 20), and the average for all wells was 61 Mcf/d.

Generally, BYG is greater in the northeast 2/3 of Garden Plains field (> 50 Mcf/d) than in the west and southwest 1/3 of the field (generally, BYG < 30 Mcf/d) (Fig. 19d). BYG exceeds 50 Mcf/d and commonly is greater than 100 Mcf/d in an east-trending belt along the northwest margin of the field (Fig. 19d, Area A). In the center of the field, the 50 Mcf/d contour encloses higher producing wells that, in the south form a northeast-trending pattern and on the north have a strongly developed, east-trending pattern (Fig. 19d, areas B1 and B2, respectively). Three areas of high BYG that occur along the southeast margin of the field (Fig. 19d, Areas C, D, and E) result from a total of 4 data points, and the 2 bulls-eye patterns in the south part of the field (Fig. 19d, Areas F and G) result from one data point each. Thus, areas C-G are production anomalies that should be further investigated to determine whether they are due to either (a) anomalous reservoir

character, such as natural fractures, or (b) erroneous data. These areas were not considered in our evaluation of geologic controls on gas production in the next section.

Geologic Controls on Gas Production

Structural Controls. Elevation of the SSPK is highest (>40 ft [12 m] above SL) along the northeast margin of the field (T33-34N, R11W), which is an area of low to intermediate BYG. Structural position does not appear to be the sole determinant of reservoir performance. However, as noted above, wells in the structurally high east and northeast 2/3 of the field have relatively high BYG (30-120 Mcf/d) in comparison to the structurally low west and southwest areas of Garden Plains field, where generally, BYG is <30 Mcf/d (Fig. 8 and Fig. 19d). Moreover, preliminary analysis indicates higher water/gas ratios in the west and southwest areas.[12] In several cases, local areas of high BYG appear to coincide with subtle structural closures having approximately 20 ft (6 m) of relief. These small structural closure and the west-trending syncline formed after deposition of Units A and B and during deposition of Units C and D, as demonstrated in isopach maps (Fig. 10a to Fig. 10d). It is unclear whether the small closures are small folds or minor faults that may result in fracture-enhanced permeability or, possibly, products of soft-sediment deformation.

Porosity-Net-Thickness Product. High BYG values in areas B1 and B2 of Garden Plains field coincide with regions of greater than average net-sandstone thickness and high porosity-net-thickness product of Unit A and Units A+B (Fig. 17a and Fig. 17c, Fig. 19c, and Fig. 19d). It appears that net thickness of Units A+B (especially net thickness of Unit A) exercises primary control on gas production. However, the highest BYG occurs in an east-trending belt of along the northwest margin of the field (Fig. 19d, area A). This is an area of lower porosity-net-thickness product (Fig. 19c), but it is the site of the earliest wells in the field [12] and may indicate higher production associated with high initial reservoir pressures. The east-trending area of low BYG between Areas A and B1 (Fig. 19d) coincides with low permeability (Fig. 19b).

Validation with Garden Plains (SSPK) Field

In this section we present the validation of the improved simulation-based regression technology in the Garden Plains SSPK reservoir. Garden Plains SSPK field has produced for 26 years since its first gas well was put on production in April 1979. Based on available field data, there are 772 gas wells producing only from the Second White Specks (SSPK) formation, and most of the wells (approximate 71%) were completed after 2001. The study area is about 492,000 acres. We use a simulation grid with 1232-ft by 1232-ft gridblocks. Well locations are shown superimposed on the simulation grid in Fig. 21.

The validation was conducted by withholding the last two years of production from the history match. After history matching, a 2-year performance prediction was made and

compared to the actual last two years of production for validation. The first 618 existing wells (pink dots, Fig. 21) were used for history matching, whereas the 154 wells drilled after 2002 (blue dots) were considered to be infill wells for validation of performance predictions.

VALIDATION OF OTHER MODEL IMPROVEMENTS

We first investigated the impact of secondary improvements made to the infill assessment technology discussed above, e.g., better modeling of hydraulically fractured well productivities and incorporation of days-on-line information. To demonstrate the impact of these improvements, we ran the new reservoir model, initializing with a homogeneous model and performing the inversion on permeability only ─ similar conditions at which the previous model was run. The results from the previous reservoir model and the new model are compared in terms of the errors of calculated production data relative to the observed data. Table 1 shows the relative errors of cumulative production for field-wide and individual wells. The prediction errors with the new model have been significantly reduced for both existing and infill wells. For example, the error for infill wells on a field-wide basis dropped to 3.38% from 65%. Similar results are seen for average and median errors on an individual-well basis. To further highlight the improvement, we note that the errors in Table 1 presented using the previous simulator exclude the wells with outlier results while those errors using the new simulator have not. It is clear that the new simulator can forecast production and remaining reserves much more reliably than the previous simulator.

Table 1—Comparison between the previous simulator and the revised simulator running inversion on permeability only: relative error of predicted cumulative production for Garden Plains gas field

Relative error, %	Existing wells		Infill wells	
	Previous simulator	New simulator	Previous simulator	New simulator
Field wide	37.42*	7.63	65.26*	3.38
Individual well average	46.41*	38.72	113.06*	31.3
Individual well median	37.93*	10.57	94.46*	24.76

* Wells with outlier results were excluded.

VALIDATION OF SEQUENTIAL INVERSION TECHNIQUE WITH A PRIOR GEOLOGICAL MODEL

To illustrate improvement gained with our new sequential inversion technique in the Garden Plains SSPK reservoir, we compared the differences in simulation results of history matching and prediction with inversion of permeability only to results generated with inversion of both permeability and pore volume. In this analysis, we started the regression with a prior geological model obtained from a detailed geological study of the Garden Plains SSPK reservoir. Results are shown in terms of both field-wide cumulative production plots (Fig. 22) and field-wide daily production rate plots (Fig. 23). The calculated results based on inversion of permeability only are shown with green lines, and the results from inversion of both permeability and pore volume are shown with red lines. For comparison, the actual rate and cumulative production observed are also displayed in these figures with blue lines. The duration of history matching is from 1979 to 2002. We predicted infill drilling performance from the beginning of 2003, as indicated by a vertical dashed line, up to the end of 2004. From these figures, it is obvious that inversion of both permeability and pore volume provides much more reliable prediction than inversion of permeability only.

Comparison of predicted cumulative production for existing and infill well groups is shown in Fig. 24. The upper set of curves is for the group of existing wells, and the lower set of curves is for the infill well group. These results also indicate that predicted production from inversion of both permeability and pore volume is much closer to actual observed production, compared with predictions from inversion of permeability only.

Table 2 lists some statistics that quantify these improvements in predicted production. The relative error on a group-wide basis for existing wells is 4.98% from inversion of both permeability and pore volume compared to 17.71% from inversion of permeability only. For infill wells, the relative errors are -5.79% versus 17.88%, respectively. Similar comparative results were observed on an individual-well basis. These results further demonstrate that inversion of both permeability and pore volume provides more reliable history matching and prediction than inversion of permeability alone.

Table 2—Relative error of predicted cumulative production for Garden Plains gas field

Relative Error, %	Existing wells		Infill wells	
	Perm only	Perm + Pore Vol.	Perm only	Perm + Pore Vol.
Group-wide	17.71	4.98	17.88	-5.79
Individual well average	52.85	11.09	46.00	20.16
Individual well median	18.83	5.20	39.93	4.29

APPLICABILITY OF SEQUENTIAL INVERSION TECHNIQUE WITHOUT A PRIOR GEOLOGICAL MODEL

In the analysis above, prior distributions of porosity, permeability and net thickness from a detailed geological study were used in the inverse modeling. However, in many stripper well fields, detailed geological studies cannot be justified economically. Thus, detailed geological models are often not available for assessment of infill potential in stripper well fields. This raises a question**:** Can we use the new technology described herein when a detailed prior geological model is not available and still get reasonable predictions of existing and infill well performance?

In this section, we compare the calculated production from inversion based on a homogeneous initial geological model to calculated production from inversion based on a detailed prior geological model. For the homogeneous initial model case, we started with estimated average values of permeability, porosity, net thickness, and gas saturation equal to 0.1 md, 12.9%, 15 ft and 35%, respectively. We applied our new sequential technique to invert both permeability and pore volume, and then predicted the production performance using the inverted permeability and pore volume fields.

Fig. 25 and Fig. 26 show comparisons of field cumulative production and field daily production, respectively, for both the history match and forecast periods. The case with the initial homogeneous model is shown as red lines, and the case with a detailed prior geological model is shown as green lines. Again, blue dots are the actual performance. These figures demonstrate that the results from a homogeneous initial model are very close to those starting with a detailed prior geological model. Similar results are observed when the comparisons are separated for existing wells and infill wells, as shown in Fig. 27.

The results presented in this section indicate that if a detailed prior geological model is not available, we can obtain reasonable reservoir characterization and prediction of production performance by regression of production data starting with only estimated average reservoir properties.

Assessment of Infill Drilling Potential

In this section, we apply the newly developed simulation-based regression technology to assess infill drilling potential in the Garden Plains gas field by estimating the incremental field production for each of the potential infill well locations in the field. For this analysis, the history matching is performed with all production data from all wells. Thus, we include the last two years of production, from January 2003 through December 2004, which we previously withheld for validation. A total of 772 wells was history matched in this analysis. Since two more years of performance data were included in the history match, we expect a better reservoir description to be obtained by inversion. As is shown in Fig. 28, the calculated field-wide cumulative production at the end of 2004 is closer to the observed cumulative when more production data are included in the history matching.

Fig. 29 to Fig. 31 show history match results for 6 individual wells on a daily rate basis. The first two wells drilled in this field, #1 and #2 (Fig. 29), were matched very well over their production record. Although wells #586 and #604 (Fig. 30) have short production histories, their general observed production trends are captured well by history matching. Wells #102 and #110 (Fig. 31), have longer production histories than #586 and #604; thus, more data are available for history matching. However, calculated production performance does not follow observed production trends very well. This is due in part to the large oscillations, or noise, in the observed production data of these two wells. Since the regression is performed with wells constrained at constant flowing bottomhole pressure, the regression processes generate an average production rate trend over the time span. It may be possible to improve history matching in individual wells by denoising production data so as to provide a consistent production trend for history matching; however, this was not attempted in this study. Fig. 29 to Fig. 31 illustrate that the production trends of most, but not all, wells are matched well, indicating that this rapid, cost-effective method resolves large-scale reservoir property trends well but does not always resolve the reservoir description well on a fine scale.

The inverted gas permeability distributions obtained starting with homogeneous vs. detailed prior geological models are shown in Fig. 32. Similar permeability distributions are obtained. The inverted pore volume distribution is represented by the adjusted porosity-thickness product (obtained by multiplying the inverted pore volume multiplier times the product of porosity and thickness). The inverted ϕ^*h distributions obtained starting with homogeneous vs. detailed prior geological models are exhibited in Fig. 33. Again, similar ϕ^*h distributions are obtained starting with and without a detailed prior geological model.

In addition to determining the distributions of reservoir properties (permeability and pore volume) conditioned to production data, the inversion also provides the distribution of current reservoir pressure. Fig. 34 shows the reservoir pressure distributions at the end of the history match period. Based on the data available, the initial pressure in this reservoir was estimated to be approximately 957 psi. The bottomhole flowing pressure was specified in the simulation to be 250 psi, based on experience with other nearby fields. As can be seen in Fig. 34, the center and northern areas show signs of pressure depletion, whereas other areas remain near original reservoir pressure.

With the inverted permeability and pore volume distributions and the reservoir pressure distribution at the end of history, we then predict future production performance and evaluate infill well potential. Since the inversion resolves large-scale reservoir property trends well, but not always fine-scale trends, we would expect the method to accurately identify areas of the field with potential for infill drilling, but not necessarily to identify individual infill well locations. Fig. 35 shows the infill drilling incremental field production maps for the cases with the homogeneous initial model and the detailed prior geological model. Infill potential was assessed for a two-year period following the end of the history match. The number on the scale bar represents field incremental gas production per infill well over the two-year period. The trends in incremental gas

production using the homogeneous initial model are quite consistent with those using the detailed prior geological model, except for regions far from well control. Comparing the distributions of reservoir properties, reservoir pressure, and infill incremental gas production, we see that areas with high infill potential do not coincide simply with areas of greater porosity and permeability or areas with higher pressure, but with a complex combination of reservoir properties, pressure and proximity to existing wells.

The results presented in this section indicate that we can obtain reasonable infill well performance prediction by integration of production data starting with only estimated average reservoir properties. Since the simulation-based regression technique can be applied using only readily available data, it is cost effective. Because the technique is approximate in that it identifies large-scale reservoir property trends, it identifies areas of the field, rather than individual well locations, that have greater potential for infill drilling. Once infill drilling in these areas is justified with economic analysis, operators can proceed with subsequent detailed analysis in these specific areas to identify individual infill well locations. Or, they can proceed with a statistical infill drilling development, i.e., blanket infill drilling in an area knowing that there may be significant variability in individual-well performance, but with the expectation that, overall, infill drilling will be profitable.

The advanced simulation-based regression technology is also rapid. For the Garden Plains field case, which has over 14,000 gridblocks and thus over 28,000 parameters, one regression run of both permeability and pore volume (3 iterations for each) requires 1.5 hours of CPU time on a desktop PC. Thus, the technology described herein can be a valuable tool for rapid and cost-effective assessment of infill and recompletion potential in stripper well gas fields in which only well locations, production data, and basic geological data (such as average porosity, thickness and permeability) are available. We believe that this advanced technology is practical and is applicable to a wide range of tight, marginal gas reservoirs.

CONCLUSIONS

1. The advanced simulation-based regression technology described herein can rapidly, reliably and cost-effectively assess infill drilling potential in stripper gas fields with large numbers of wells. It uses very basic reservoir information (such as average porosity, thickness and permeability), well locations and production data to invert both permeability and pore volume distributions, which are then used to assess infill drilling potential.
2. In synthetic cases, the improved technology was able to reproduce the main features of heterogeneous porosity-thickness and permeability distributions. Including inversion of porosity-thickness with the permeability inversion results in a significant reduction in errors in predicted performance of both existing and infill wells, as compared to inversion of permeability only as in the previous technology.
3. For purposes of validating the enhanced simulation-based regression technology, we performed a reservoir characterization study of the Garden Plains Second White

Specks reservoir. Garden plains is a stripper gas field with 772 non-commingled SSPK wells as of December 31, 2004. The average of the best year of production for all 772 wells was 61 Mcf/d. Cumulative gas production from the Garden Plains SSPK reservoir was 45.9 Bcf through December 31, 2004.

4. The lowermost units (A and B) of the SSPK formation are the primary gas-producing intervals and are the focus of this research. Units A and B were deposited as northeast-trending, very fine-grained, shaly sandstones. Net thickness of Units A+B ranges from 10.5 ft to 22 ft (3.2-6.7 m) and averages 16.5 ft (5 m). Both porosity and permeability vary laterally, indicating high lateral reservoir heterogeneity.
5. Evaluation of SSPK core data demonstrated a good relation between porosity and permeability. Porosity-net-thickness product, and by relation permeability, appear to exert the greatest control on production from SSPK reservoirs in Garden Plains field. Structural position, minor structural features, and spud date (initial reservoir pressure) exercise secondary control on production.
6. In validating the new simulation-based regression technology in the Garden Plains SSPK reservoir, we found that including inversion of porosity-thickness with the permeability inversion results in a significant improvement in matches of predicted performance of both existing and infill wells, as compared to inversion of permeability only as in the previous technology.
7. Inverted permeability and pore volume distributions, performance predictions and infill assessments in the Garden Plains SSPK reservoir generated starting with a homogeneous geological model were similar to property distributions, predictions and infill assessments generated starting with a detailed prior geological model. This validates the use of the technology in situations in which a detailed geological model is not available.

REFERENCES

1. McCain, W.D., et al., *A Tight Gas Field Study: Carthage (Cotton Valley) Field*, in *SPE Gas Technology Symposium*. 1993: Calgary, Alberta, Canada.
2. Voneiff, G.W. and C.L. Cipolla, *A New Approach to Large-Scale Infill Evaluations Applied to the OZONA (Canyon) Gas Sands*, in *SPE Permian Basin Oil & Gas Recovery Conference*. 1996: Midland, Texas.
3. Hudson, J.W., J.E. Jochen, and V.A. Jochen, *Practical Technique to Identify Infill Potential in Low-Permeability Gas Reservoirs Applied to the Milk River Formation in Canada*, in *SPE/CERI Gas Technology Symposium*. 2000: Calgary, Alberta, Canada.
4. Guan, L., et al., *Evaluation of a Statistical Infill Candidate Selection Technique*, in *SPE Gas Technology Symposium*. 2002: Calgary, Alberta, Canada.
5. Gao, H. and D.A. McVay, *Gas Infill Well Selection Using Rapid Inversion Methods*, in *SPE Annual Technical Conference and Exhibition*. 2004: Houston, Texas.
6. McVay, D.A., et al., *Final Report: Advanced Technology for Infill and Recompletion Candidate Well Selection*. 2004, Dept. of Energy, Stripper Well Consortium.

7. Tang, Y.N., et al., *Generalized Pulse-Spectrum Technique for 2-D and 2-Phase History Matching.* Applied Numerical Mathematics, 1989. **5**(6): p. 529-539.
8. Chu, L., A.C. Reynolds, and D.S. Oliver, *Computation of Sensitivity Coefficients for Conditioning the Permeability Field to Well-Test Pressure Data.* In Situ 1995. **19**: p. 179.
9. Lee, W.J. and R.A. Wattenbarger, *Gas Reservoir Engineering*. Textbook Series. Vol. 5. 1996, Richardson, Texas: Society of Petroleum Engineers.
10. Paige, C.C. and M.A. Saunders, *LSQR: An Algorithm for Sparse Linear Equations and Sparse Least Squares.* ACM Transactions on Mathematical Software 1982. **8**(1): p. 43.
11. Nolet, G., *Seismic Wave Propagation and Seismic Tomography*, in *Seismic Tomography: With Applications in Global Seismology and Exploration Geophysics*. 1987, Springer: New York. p. 1-23.
12. *Unpublished maps and data of Garden Plains field*. 2004, MGV Energy, Inc.
13. O'Connell, S., *The Second White Specks, Medicine Hat and Milk River Formations, a shallow gas core workshop*. 2005, Belfield Resources Inc.: Calgary.
14. Snowdon, L.R., *Rock_eval Tmax suppression: documentation and amelioration.* AAPG Bulletin, 1995. **79**(9): p. 1337-1348.
15. Bloch, J.D., et al., *Revised stratigraphy of the Lower Colorado Group (Albian to Turonian), Western Canada.* Canadian Petroleum Geology Bull., 1993. **41**: p. 325-348.
16. Leckie, D.A., et al., *Cretaceous Colorado / Alberta Group strata of the Western Canada Sedimentary Basin*, in *Geological Atlas of the Western Canada Sedimentary Basin*, G. Mossop and I. Shetsin, Editors. 1994, Canadian Society of Petroleum Geologists and Alberta Research Council: Calgary. p. Chapter 20, 335-352.
17. Schroder-Adams, C.J., et al., *Paleoenvironmental changes in the Cretaceous (Albian to Turonian) Colorado Group of western Canada: Microfossil, sedimentological and geochemical evidence.* Cretaceous Research, 1996. **17**: p. 311-365.
18. Glass, D.J., ed., *Lexicon of Canadian stratigraphy, volume 4, including Eastern British Columbia, Alberta, Saskatchewan, and Southern Manitoba*. 1990, Calgary, Alberta: Canadian Society of Petroleum Geologists. 772.
19. Creaney, S. and J. Allan, *Hydrocarbon generation and migration in the Western Canada basin*, in *Classic Petroleum Provinces*, J. Brooks, Editor. 1990, Blackwell: London. p. 129-202.
20. Portigal, M.H., et al., *Oil and gas developments in western Canada in 1987.* Bulletin of Canadian Petroleum Geology, 1989. **37**: p. 334-345.
21. Shurr, G.W. and J.L. Ridgley, *Unconventional shallow biogenic gas systems.* AAPG Bulletin, 2002. **86**(11): p. 1939-1969.
22. O'Connell, S., *The unknown giants - low-permeability shallow gas reservoirs of southern Alberta and Saskatchewan, Canada (abs.)*, in *Joint Conference of the Canadian Society of Exploration Geophysicists and Canadian Society of Petroleum Geologists*. 2003.
23. Shier, D.E., *Well log normalization: methods and guidelines.* Petrophysics, 2004.

45(3): p. 268-280.
24. Stelck, C.R., W.E. Moore, and S.G. Pemberton, *Early Turonian (Late Cretaceous) age of the Tuskoola sandstone Pine River area, northeastern British Columbia.* Canadian Journal of Earth Sciences, 2002. **39**: p. 1783-1793.
25. Williams, G.D. and C.R. Stelck, *Speculations on the Cretaceous paleography of North America*, in *The Cretaceous System in the Western Interior of North America*, W.G.E. Caldwell, Editor. 1975, Geological Association of Canada. p. 1-20.
26. Buckley, L. and R.V. Tyson, *Organic facies analysis of the Cretaceous Lower and basal Upper Colorado Group (Cretaceous), Western Canada Sedimentary Basin – a preliminary report*. 2003, Saskatchewan Geological Survey. p. 1-13.

LIST OF ACRONYMS AND ABBREVIATIONS

A = coefficient matrix
API = American Petroleum Institute
$\mathbf{b}$ = right-side vector of system of equation
BYG = best year gas; average daily gas production during the best 12 consecutive months of production
C_α = diagonal matrix for sensitivity calculation
ft = feet
GR = gamma ray
h = net thickness
J = productivity index
m = meters
md = millidarcies
$\mathbf{p}$ = vector of pseudopressure
p = pseudopressure
PHIN_E = effective neutron porosity
p_{wf} = well flowing pseudopressure
p_{sc} = pressure at standard condition
q = production rate
S_g = gas saturation
$\mathbf{S}$ = sensitivity matrix
SSPK = Second White Specks formation
T = formation temperature
T_{sc} = temperature at standard condition
Δt = timestep interval
V_p = pore volume of gridblock
V_{sh} =shale volume
$\mathbf{X}$ = vector consisting of m-th row element of A^{-1}
x = gridblock size
y = gridblock size
z = real-gas deviation factor

α = coefficient in Eqs. 5 and 6
$\boldsymbol{\beta}$ = vector of pore volume multiplier
β = pore volume multiplier

Subscripts
g = gas phase
i = index of gridblock or element in matrix
l = index of gridblock with well
p = pore
sc = standard condition
wf = wellbore flowing condition

α = coefficient in Eqs. 5 and 6

Superscripts
n = current timestep level
-1 = inverse matrix

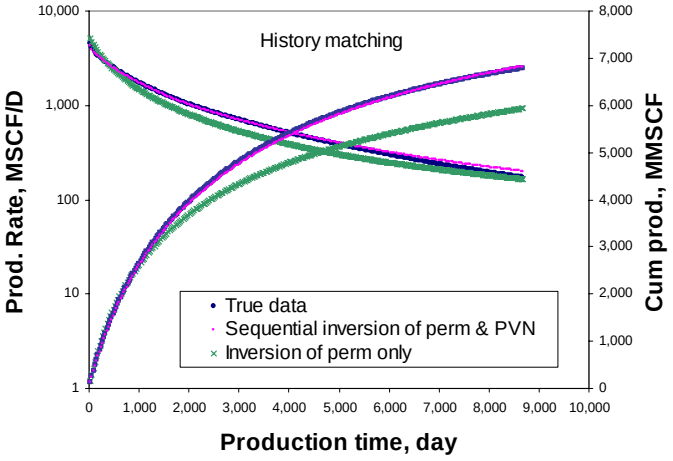

Fig. 1—History matching results for field-wide production performance.

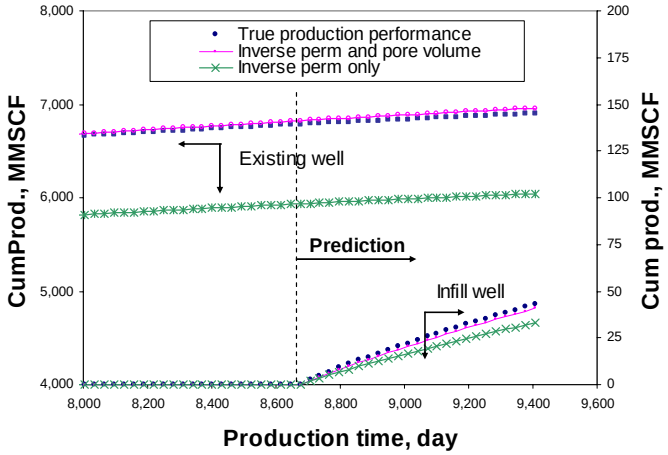

Fig. 2—Prediction effectiveness for the existing well group and infill well group.

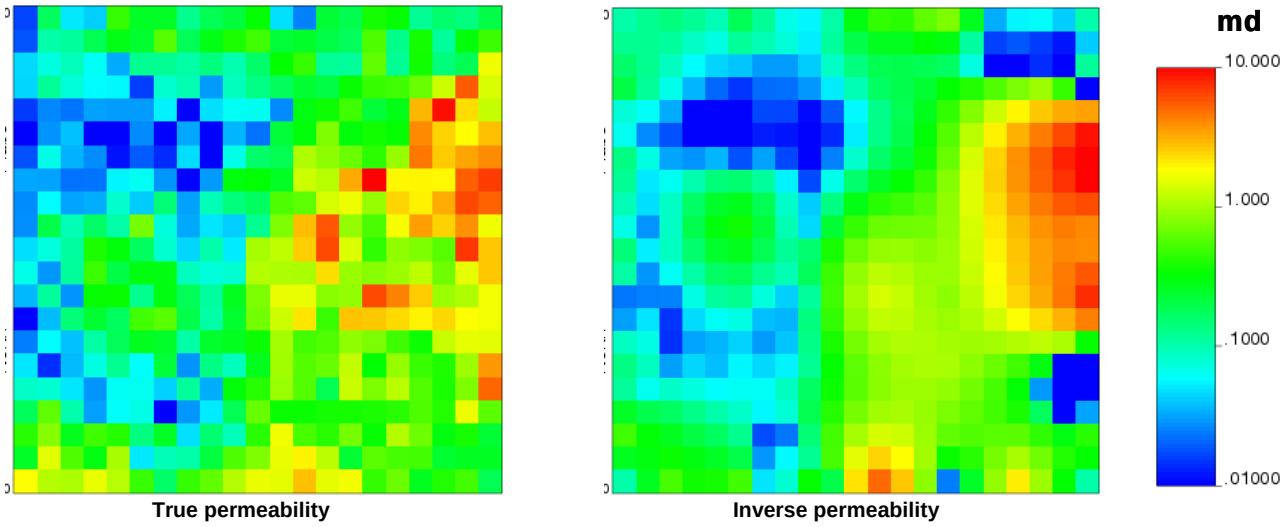

Fig. 3—Permeability distribution inverted using the sequential inversion technique vs. the true distribution.

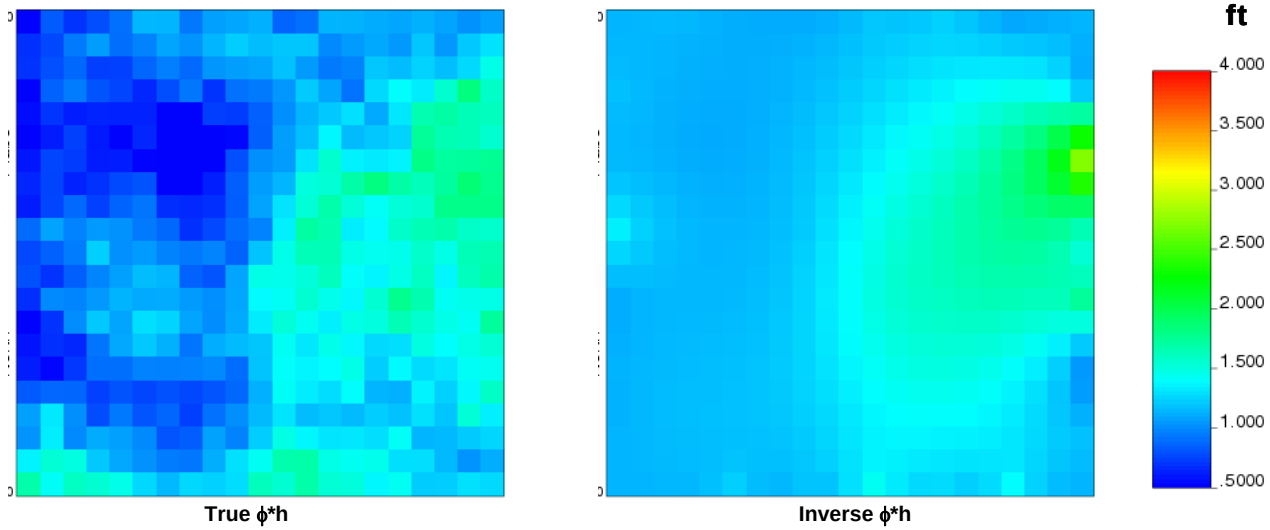

Fig. 4—phi*h distribution inverted using the sequential inversion technique vs. the true distribution.

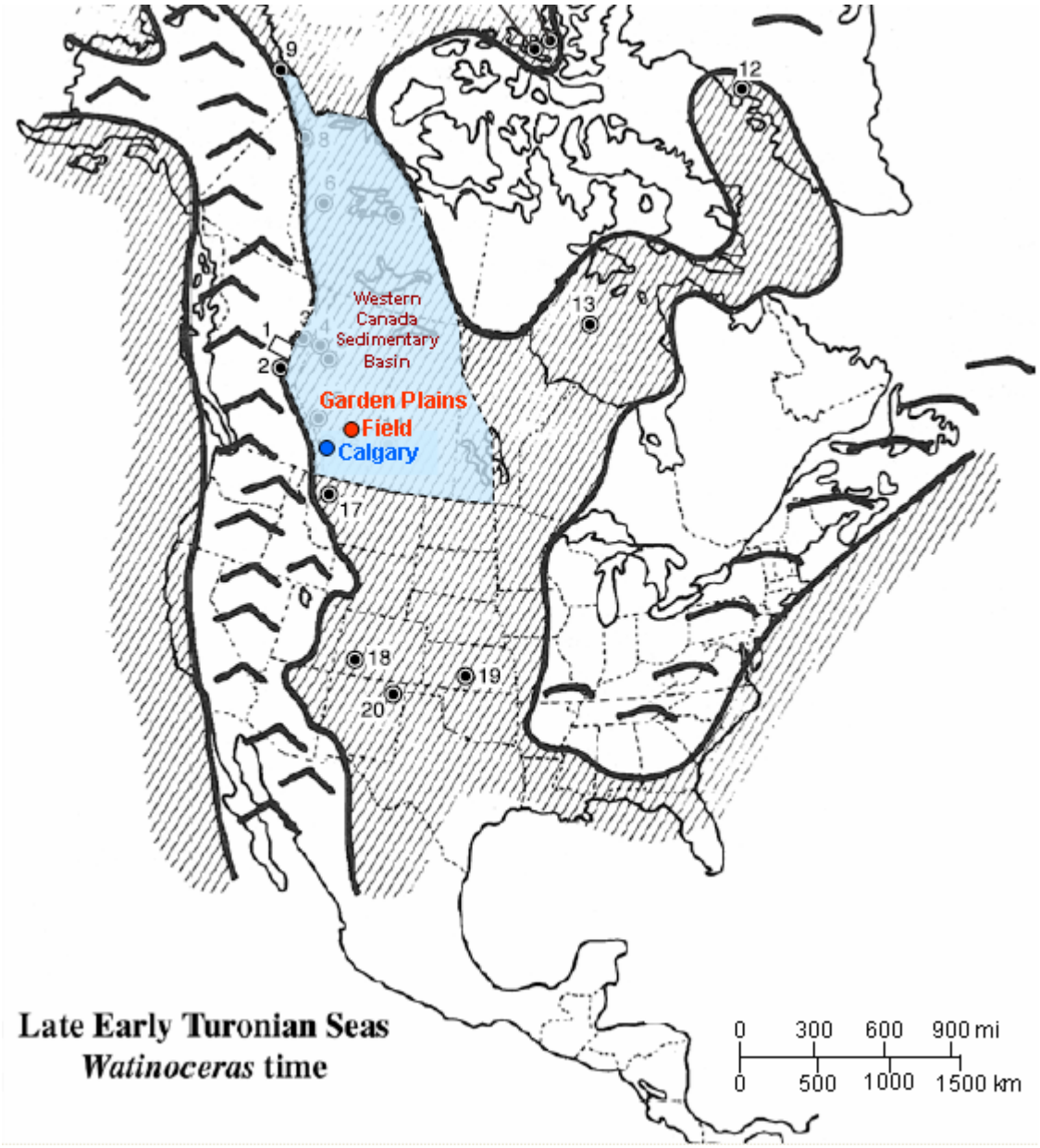

Fig. 5—Location of Garden Plains field in the Western Canada Sedimentary Basin. Base map is Turonian paleogeographical map of North America (modified from Stelck et al.[24], after Williams and Stelck[25]).

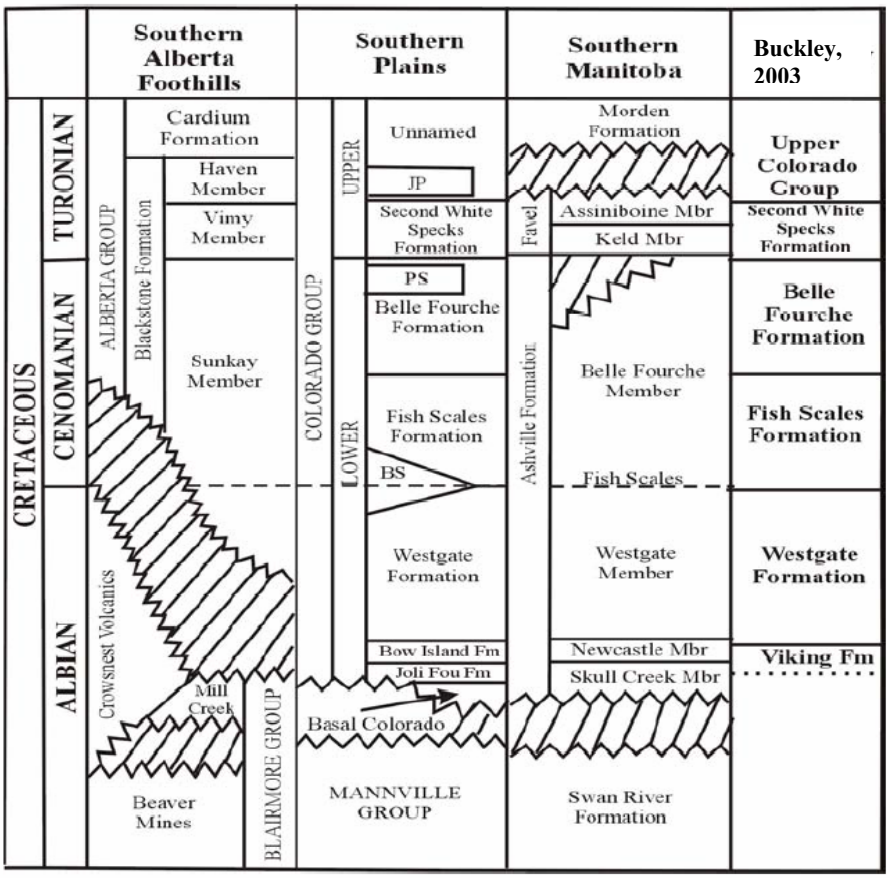

Fig. 6—Stratigraphic nomenclature of the Colorado Group in the Western Canada Sedimentary Basin (from Buckley and Tyson [26]; after Bloch et al. [15]).

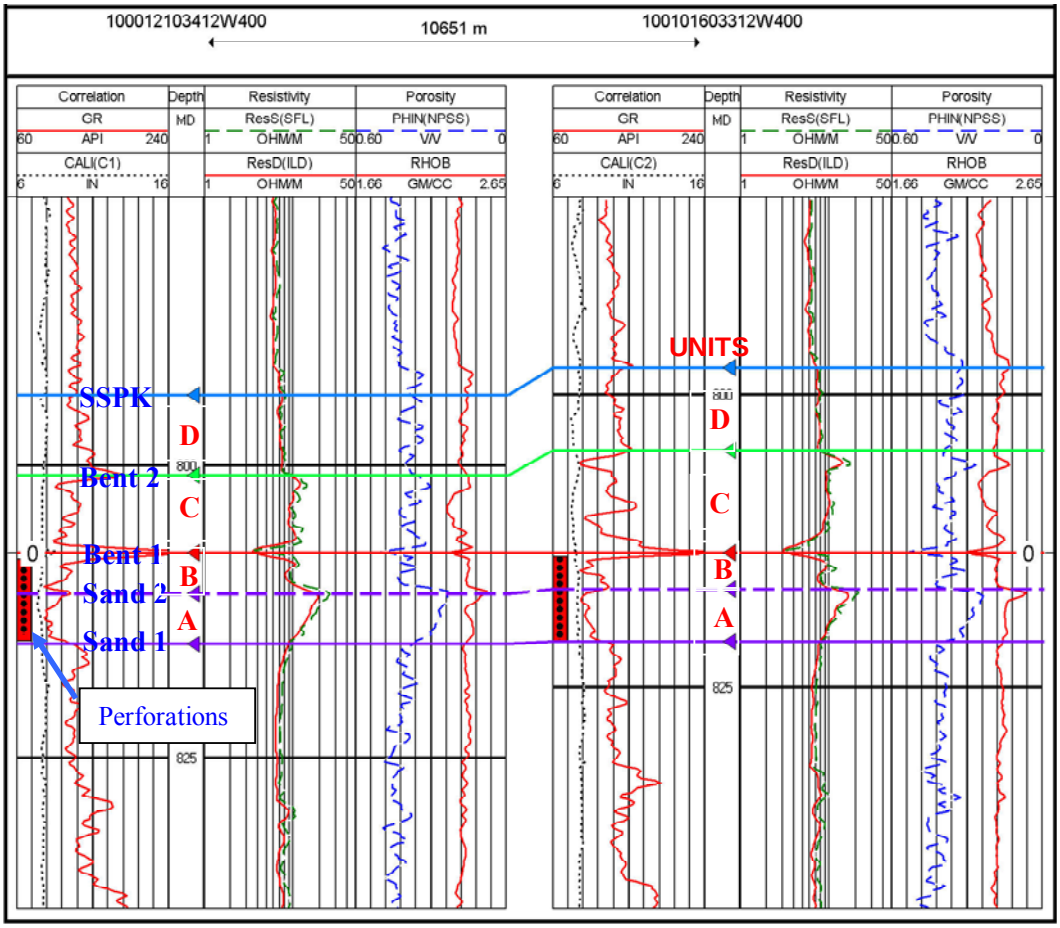

Fig. 7—Log curve response and marker beds for 2 wells in Garden Plains Field. Datum is Bentonite 1 marker bed. Sand 1 = Unit A base; Sand 2 = Unit B base; Bent 1 = Bentonite 1 and Unit C base; Bent 2 = Bentonite 2 and Unit D base; SSPK = unit D top. Gas production is primarily in Units A and B. SSPK is the top of the Second White Specks Sandstone.

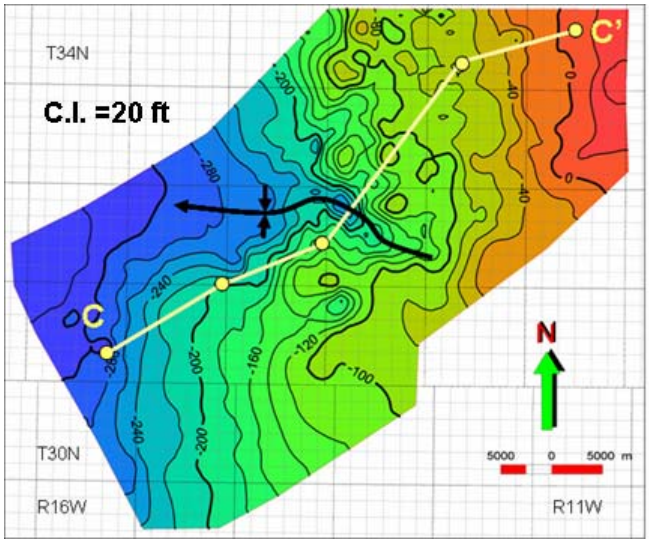

Fig. 8—Structure map of Bentonite 1, Garden Plains field. Regional dip is approximately 0.1° westward. Structural relief of the west-plunging syncline is approximately 45 m. See Fig. 7 for the stratigraphic occurrence of Bentonite 1 and Fig. 9 for cross section C-C.'

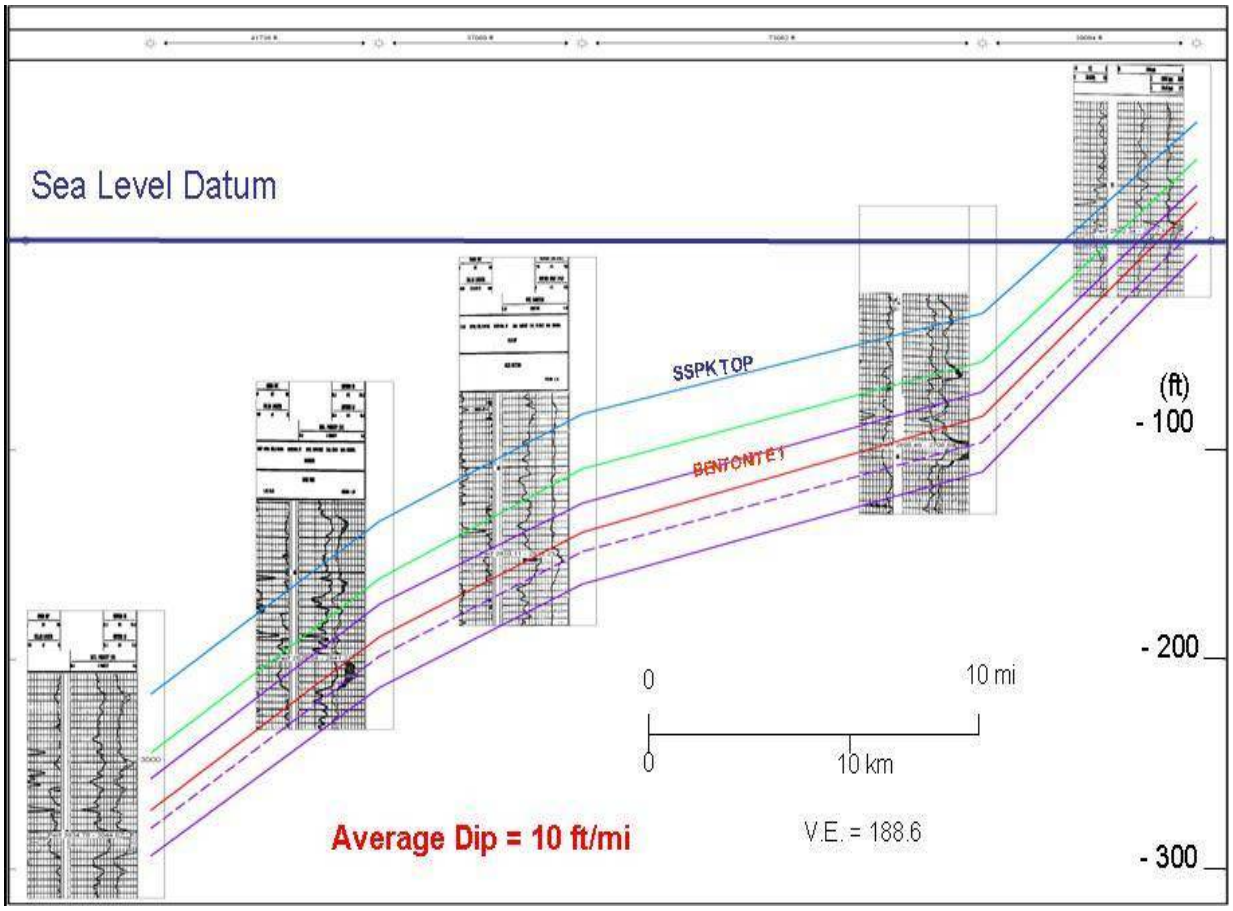

Fig. 9—Northeast-trending structural cross section C—C.' See Fig. 8 for location.

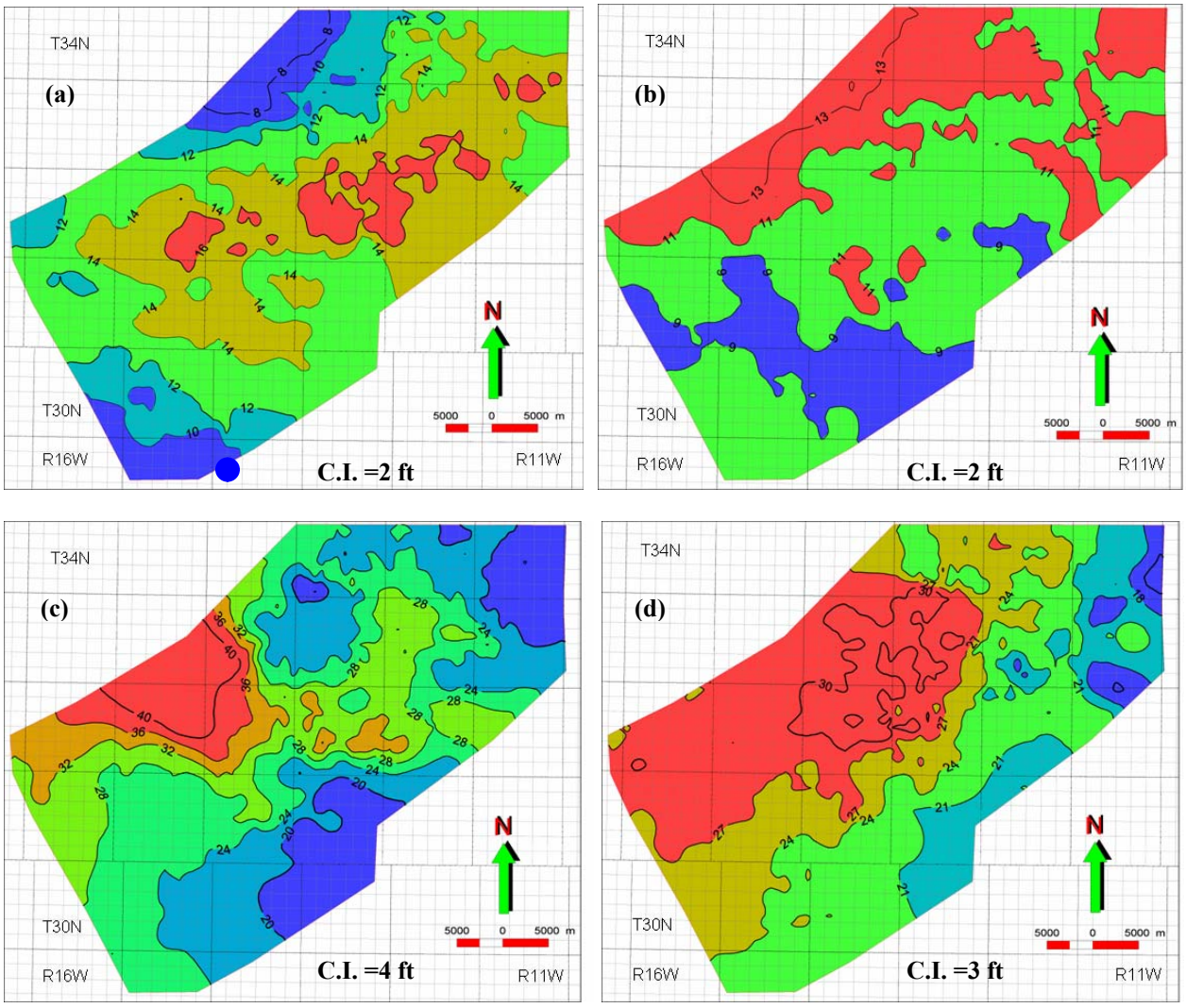

Fig. 10—Gross thickness maps for SSPK Units A- D, Garden Plains field. (a) Unit A is an upward-coarsening interval (Fig. 7) that ranges trends east-northeastward. (b) Unit B is an upward-fining interval (Fig. 7) that trends northeastward and thickens to the northwest. (c) Unit C is thickest in a west-trending area that coincides with the minor west-plunging anticline (Fig. 8). (d) Unit D trends northeastward and thickens to the northwest.

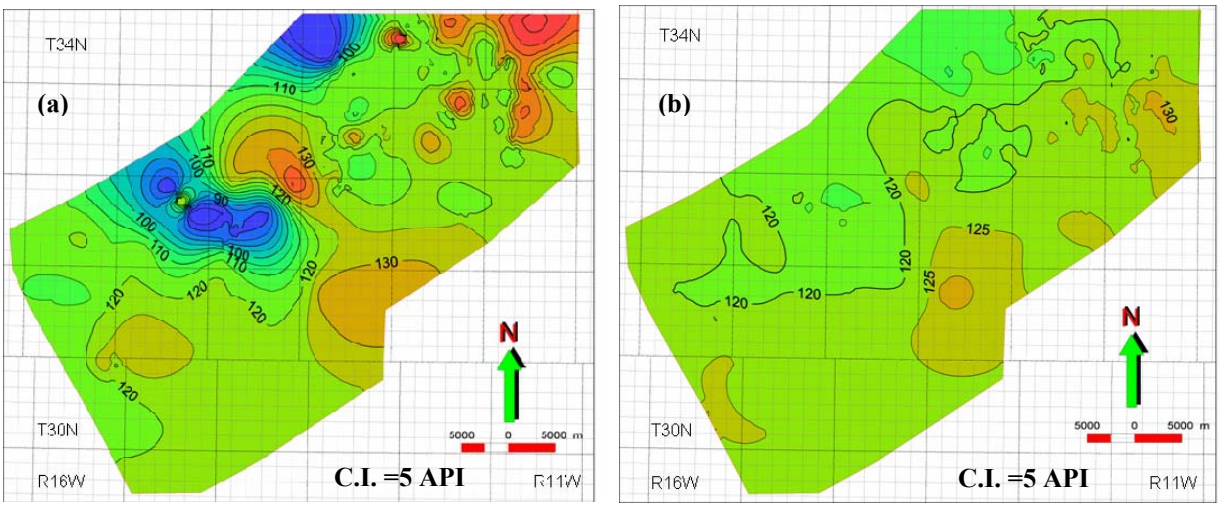

Fig. 11—(a) Average gamma ray (GR) response (API units) of Shale B before log normalization. Great variability and range of values GR values in this marine shale suggest the need for log normalization. (b) Average GR response of Shale B after normalization.

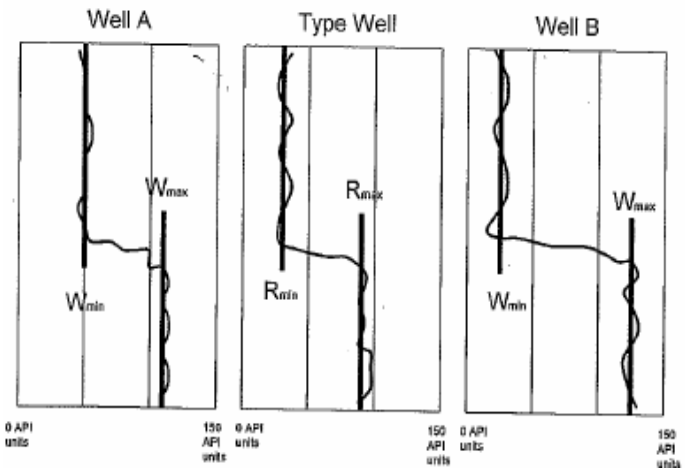

Fig. 12—Normalization parameters for GR curves (from Shier [23]).

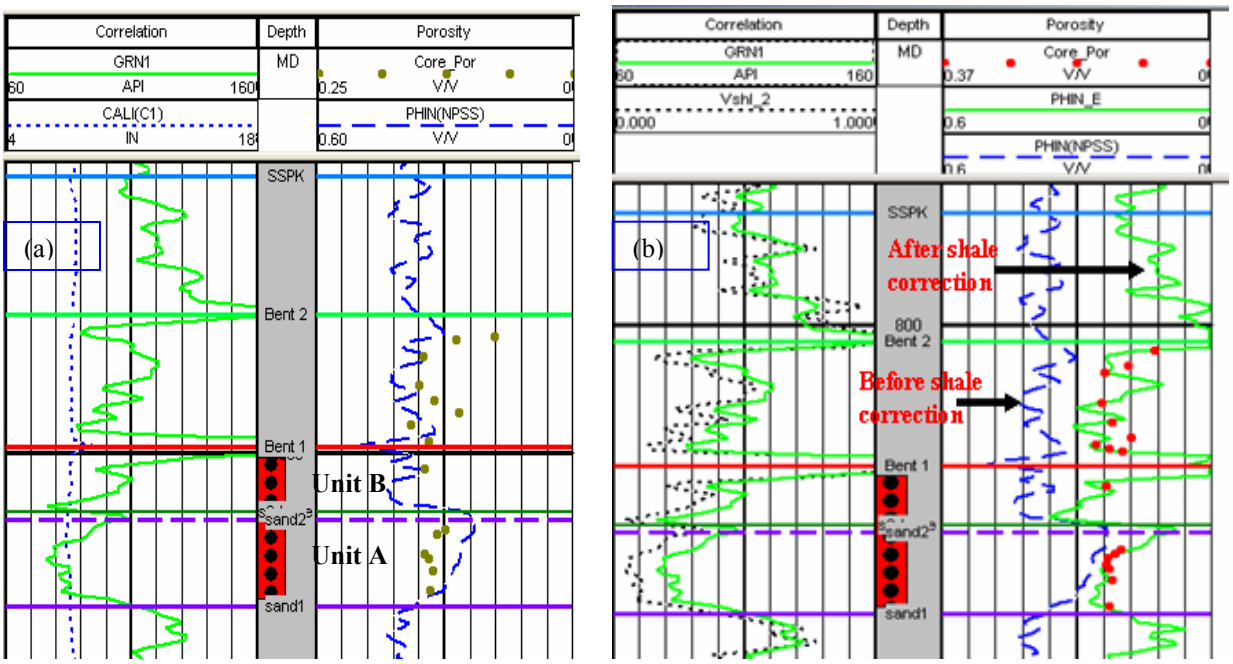

Fig. 13—(a) Core porosity vs. neutron porosity for well 100012103412W4, before depth shift. Owing to a shale effect, core porosity does not match neutron porosity. Note the difference in scales for core and neutron porosity. (b) Core porosity vs. effective neutron porosity for well 100012103412W4 after shale correction and depth shift.

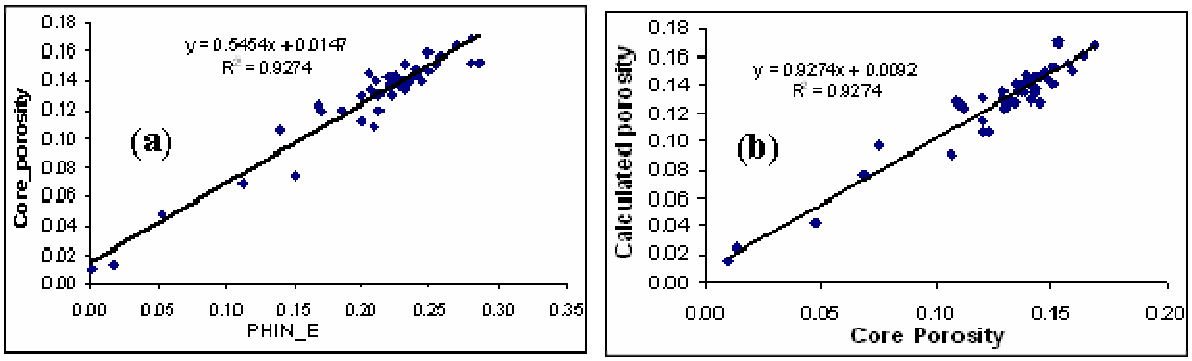

Fig. 14—(a) Core porosity vs. effective neutron porosity after shaliness correction and depth shift. (b) Plot of core porosity vs. porosity calculated using logs corrected for shaliness and depth.

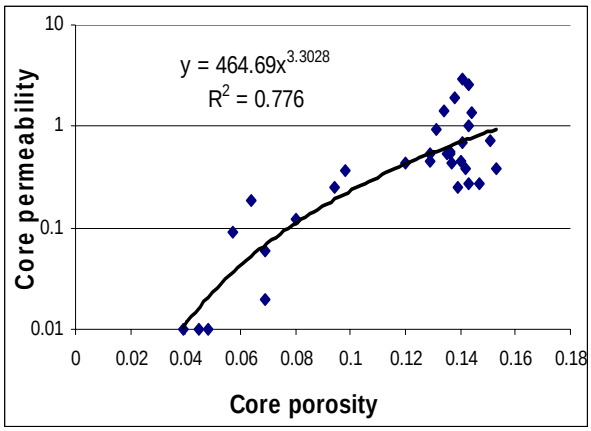

Fig. 15—Core porosity vs. core permeability, SSPK formation.

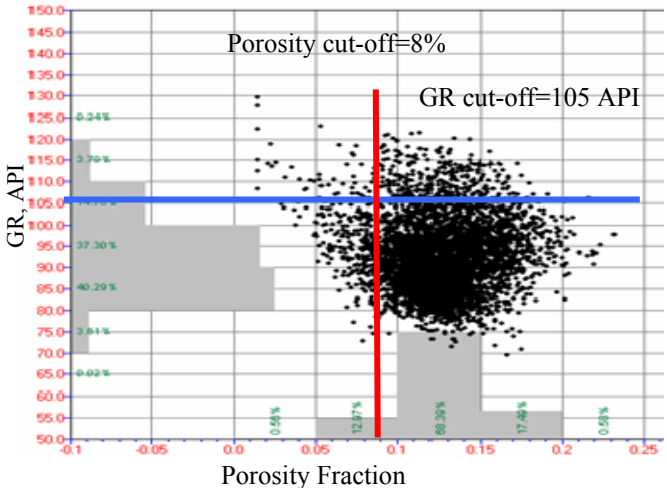

Fig. 16—Determination of net sand cutoffs of 8% porosity and gamma ray of 105 API units, Unit A.

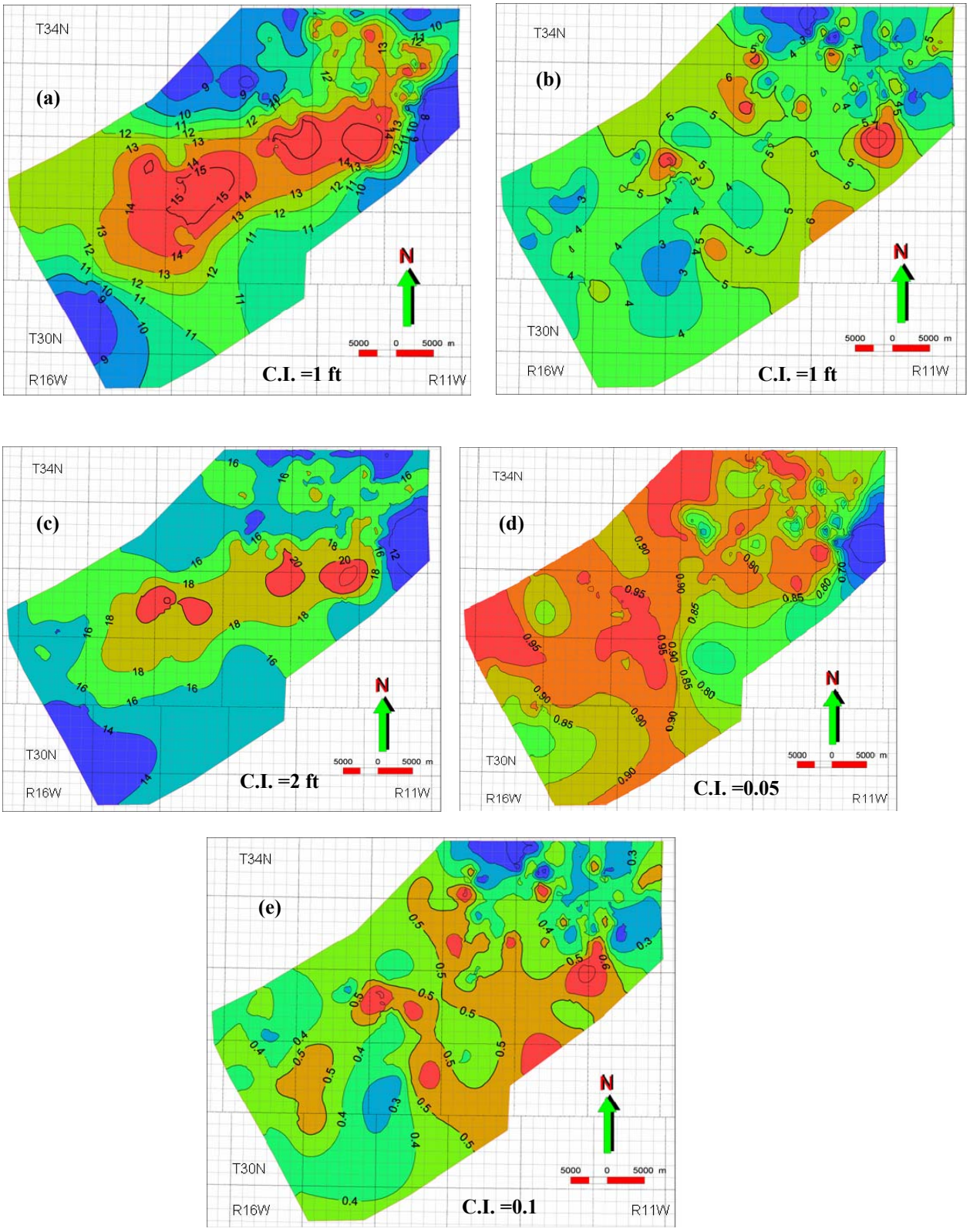

Fig. 17—Net-sandstone thickness (ft) of SSPK Unit A (a) and Unit B (b). (c) Net-sandstone thickness (ft) of Units A+B. Net/gross ratio of Unit A (d) and Unit B (e).

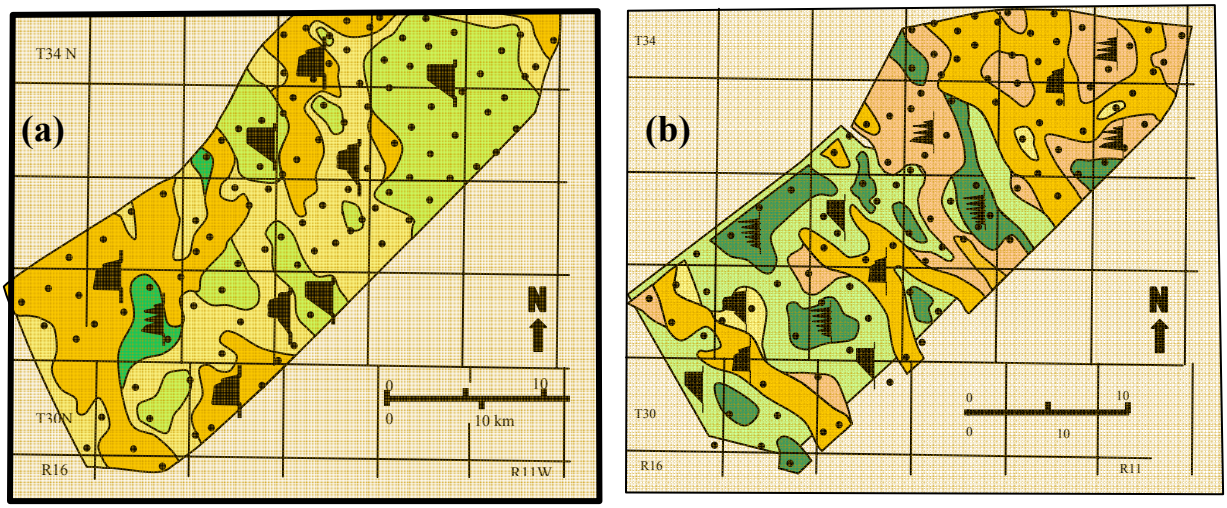

Fig. 18—Well-log patterns/facies for SSPK Unit A (a) and Unit B (b). Generally, log facies are complex and trend northwestward. Log pattern classification is shown below with a numerical classification that is sometimes used for computer contouring.

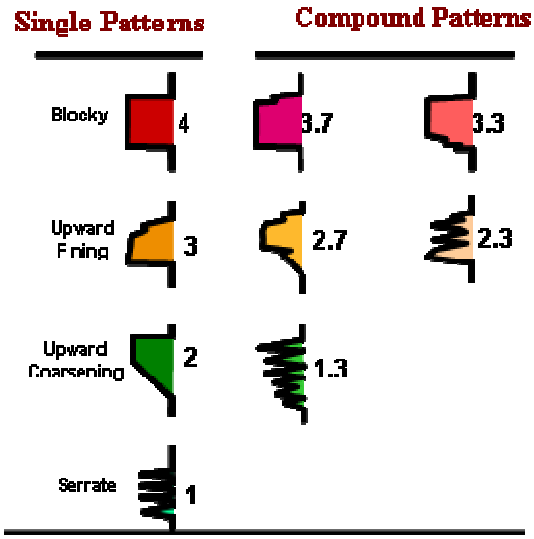

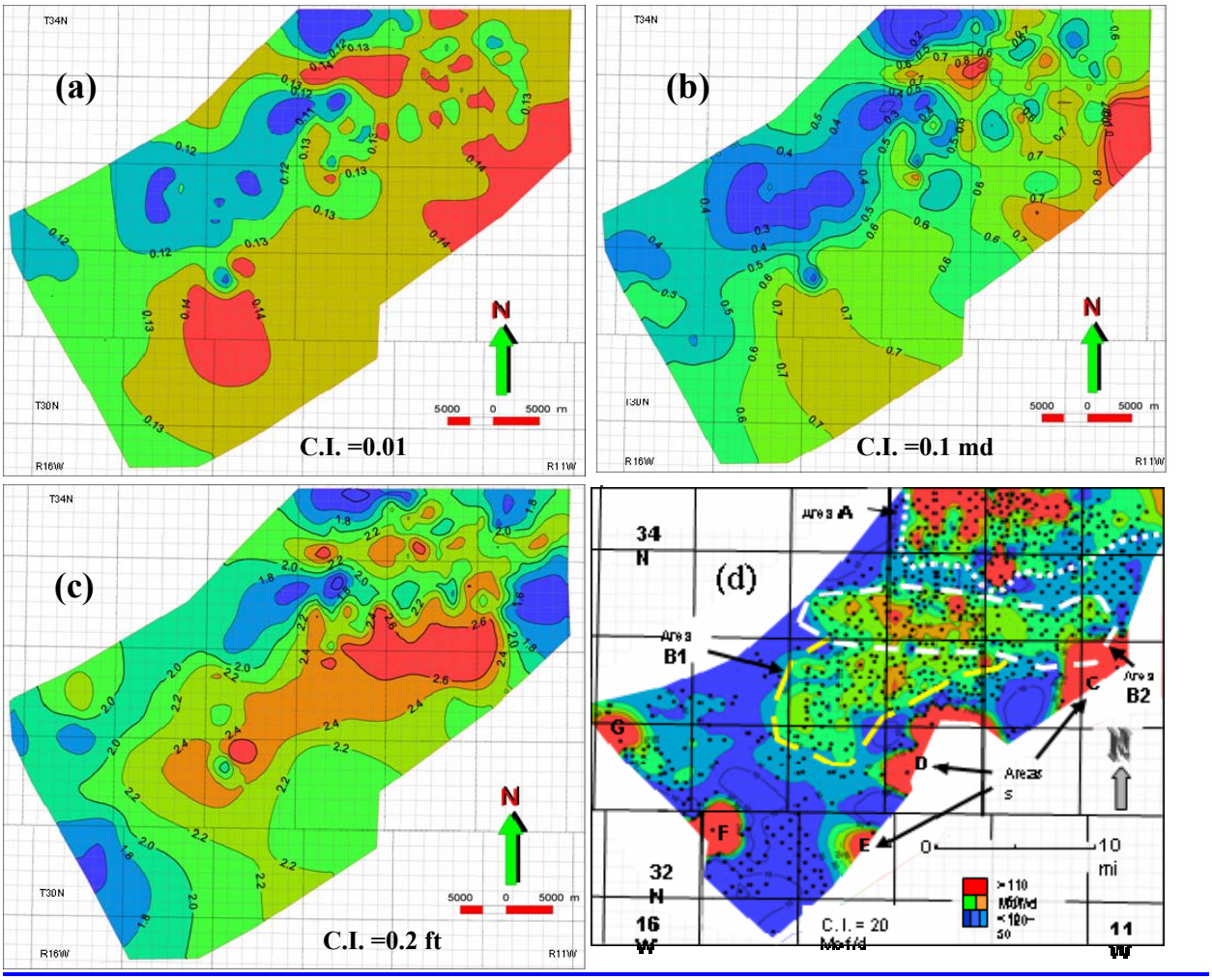

Fig. 19—(a) Average porosity and (b) average permeability (md) of SSPK Units A+B. (c) Porosity-thickness product of SSPK Units A+B. (d) Best year production of SSPK reservoir in Garden Plains field. Best year production is defined as average daily production during the best 12 consecutive months of production.

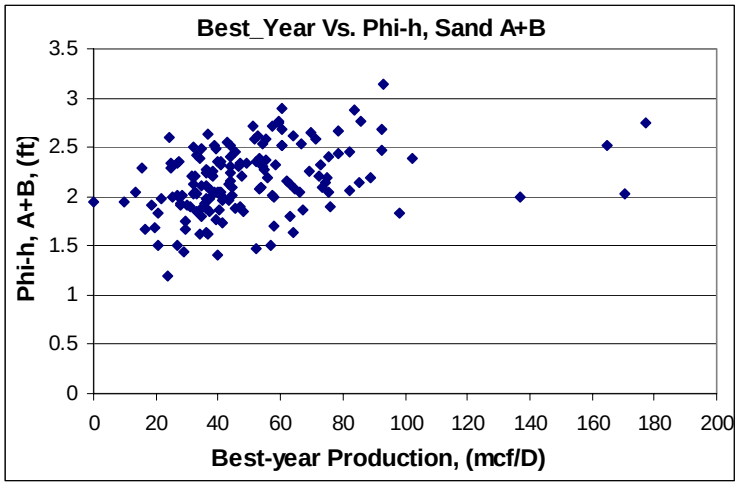

Fig. 20—Porosity-thickness product of Units A+B vs. best year production.

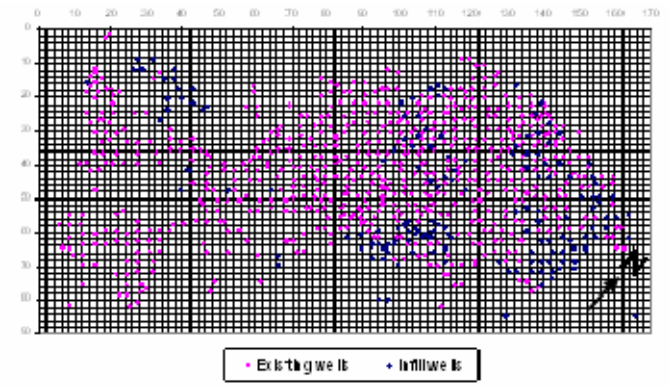

Fig. 21—Garden Plains field well location.

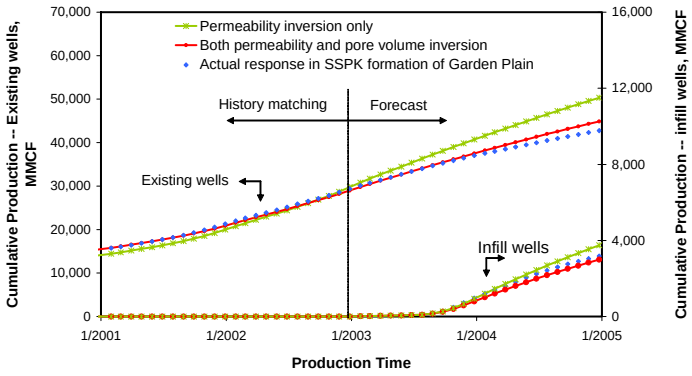

Fig. 24—Prediction results for existing well group and infill well group for Garden Plains field.

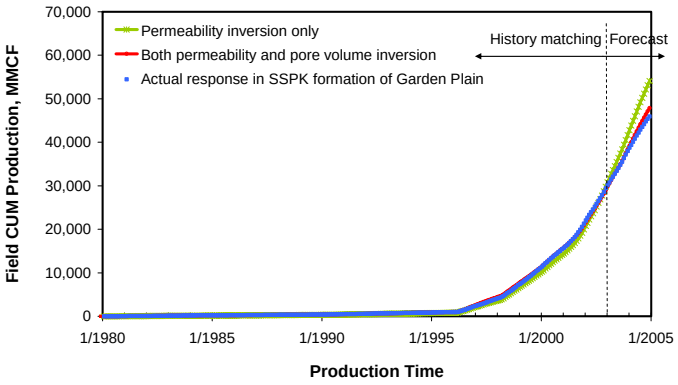

Fig. 22—History match and forecast of cumulative production for Garden Plains field, with detailed prior geological model.

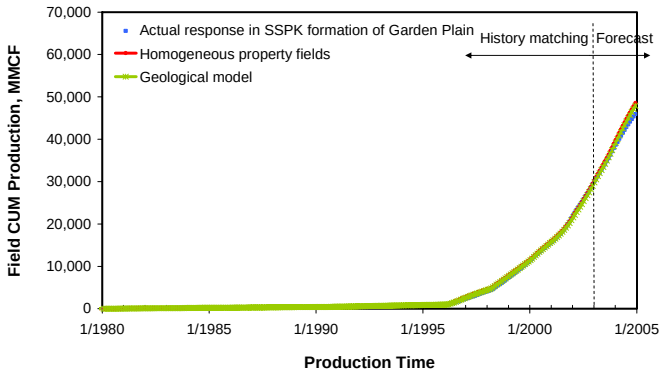

Fig. 25—Comparison of field cumulative production of Garden Plains field using homogeneous vs. detailed prior geological models.

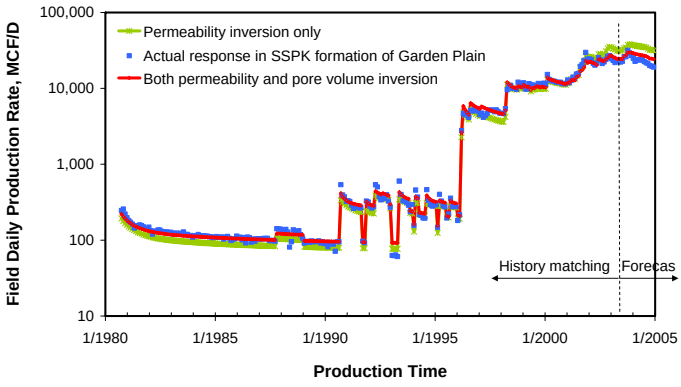

Fig. 23—History match and forecast of daily production rate for Garden Plains field, with detailed prior geological model.

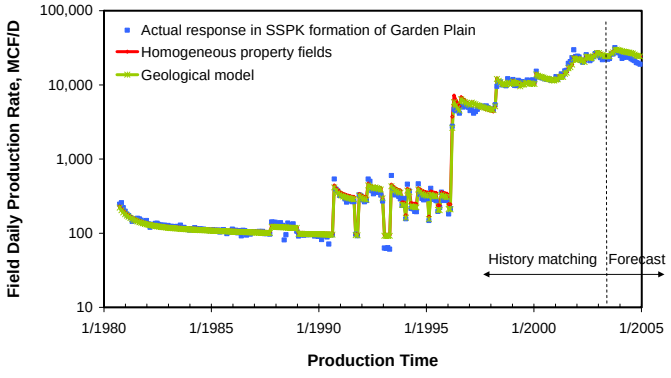

Fig. 26—Comparison of field daily production of Garden Plains field using homogeneous vs. detailed prior geological models.

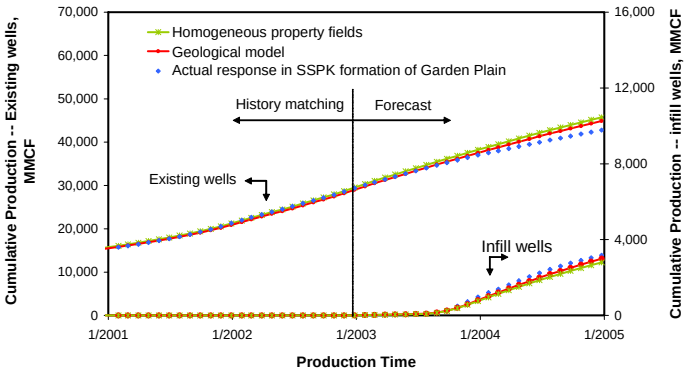

Fig. 27—Comparison of cumulative production of Garden Plains field using homogeneous vs. detailed prior geological models, for existing and infill well groups.

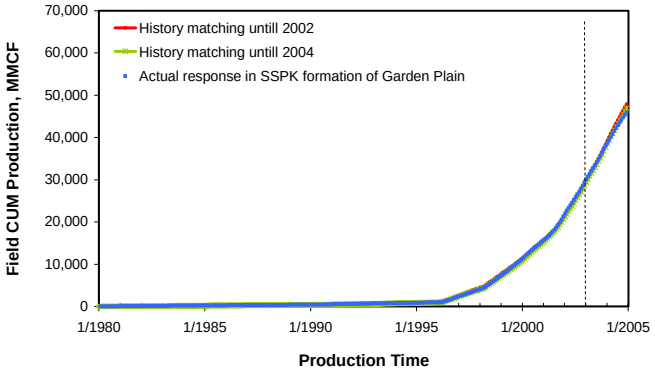

Fig. 28—History matching on cumulative production of Garden Plains field through 2002 and through 2004.

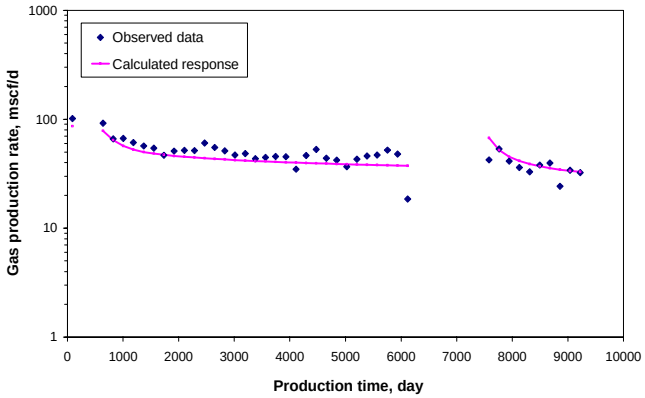

Well #1

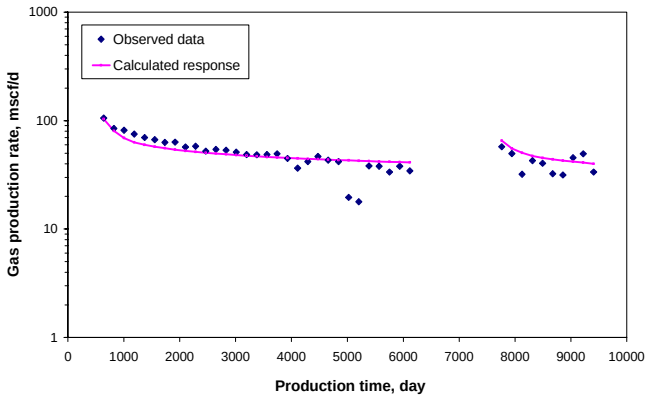

Well #2

Fig. 29—History match results for Wells #1 and #2 of Garden Plains field.

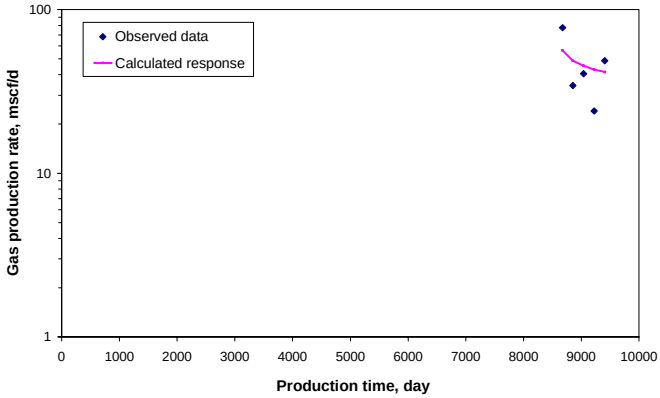

Well #586

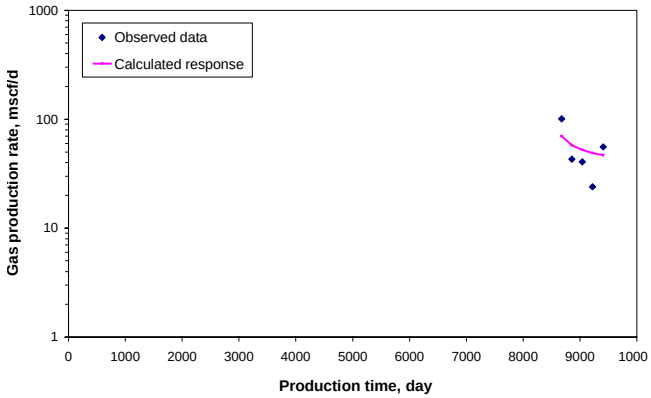

Well #604

Fig. 30—History match results for Wells #586 and #604 of Garden Plains field.

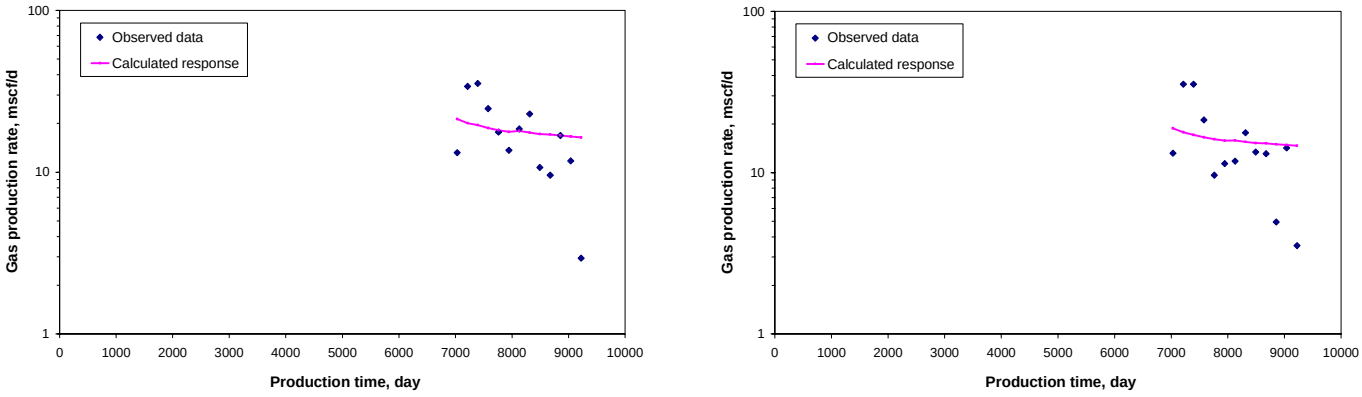

Well #102 Well #110

Fig. 31—History match results for Wells #102 and #110 of Garden Plains field.

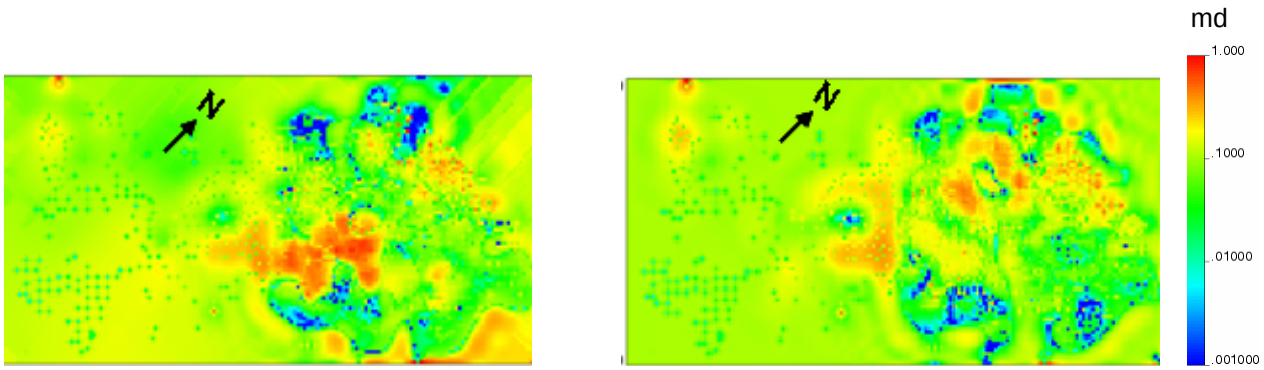

Prior geological model Initial homogeneous model

Fig. 32—Inverted permeability distribution for Garden Plains field.

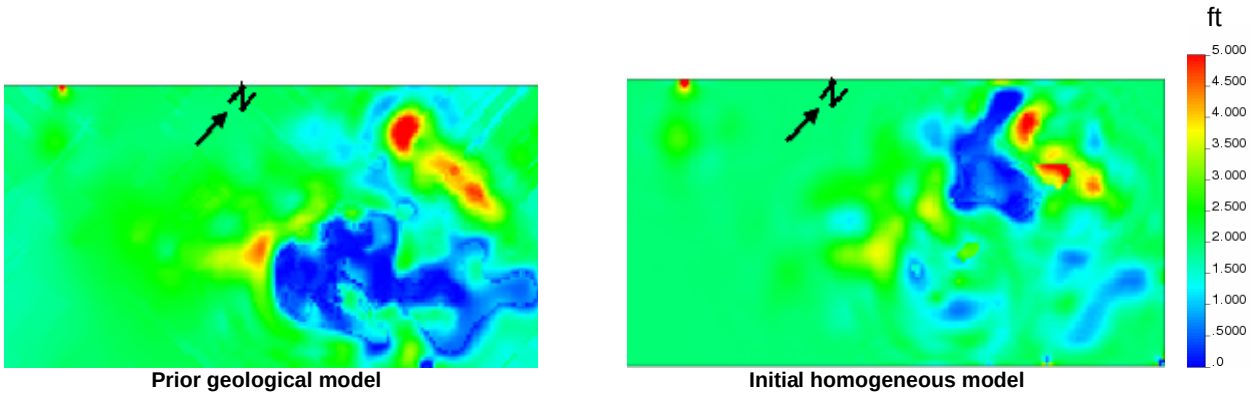

Prior geological model Initial homogeneous model

Fig. 33—Inverted phi*h distribution for Garden Plains field.

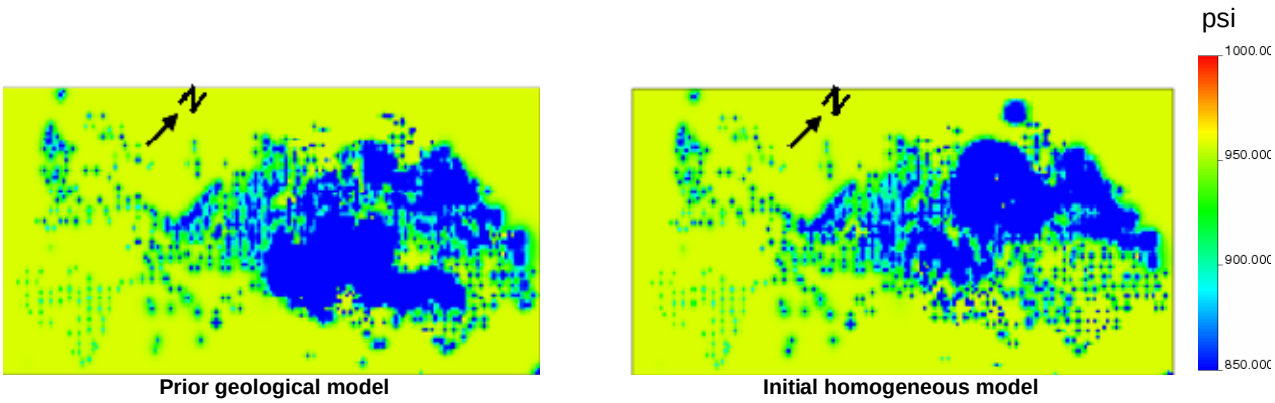

Fig. 34—Current pressure distribution of Garden Plains field.

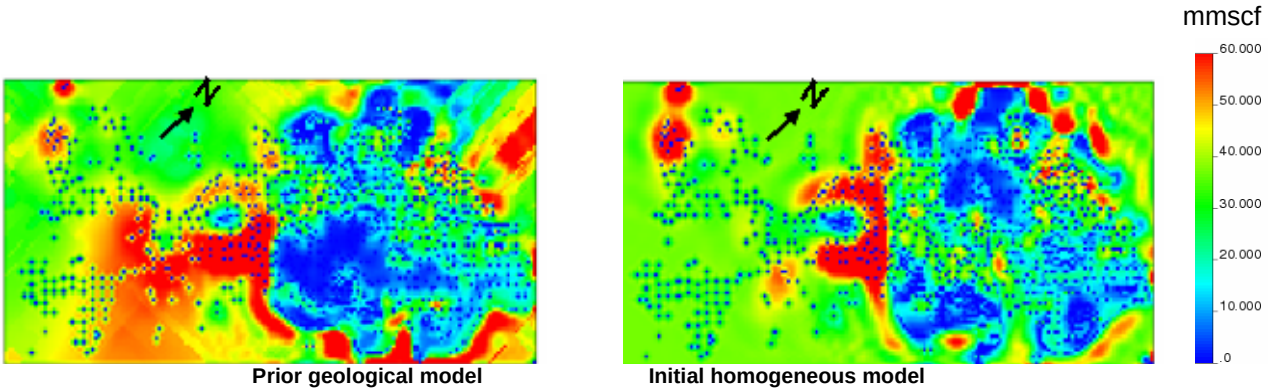

Fig. 35—Incremental field production for infill wells in the Garden Plains field.